NUMERICAL STUDY OF PNEUMATIC CONVEYING OF POWDERS

by
Muhammad Mushahid Rafique Qureshi

A Thesis
Submitted to the Faculty of
New Jersey Institute of Technology
In Partial Fulfillment of the Requirements for the Degree of
Master of Science in Mechanical Engineering

Department of Mechanical Engineering

January 2003

ABSTRACT

NUMERICAL STUDY OF PNEUMATIC CONVEYING OF POWDERS

by
Muhammad Mushahid Rafique Qureshi

The dense phase mode may be advantageous over the dilute phase mode, for some pneumatic conveying problems, because it causes less erosion of the pipeline, less attrition of the material, requires less dust collection and is effective even for smaller pipe diameters. The objective of this study is to numerically determine the parameters that govern the formation slugs in dense phase conveying. The distributed Lagrange multiplier/fictitious domain method (Glowinski et al. 1998 and Singh et al. 2000) is used to perform direct simulations of the motion of solid and gas phases in pipes with rectangular cross-sections. In this approach the exact governing equations are solved at scales finer than the particle size and no ad hoc two-phase flow model is used. Simulations are started by placing a particle slug in the flow. Several cases were simulated to understand the role of gravity, the particle density and the strength of applied pressure gradient in the formation and destruction of slugs. When the applied pressure gradient is increased the slugs become more compact, their velocity in the flow direction increases and they remain intact for longer time durations. A reduction in the pressure gradient, on the other hand, causes the particle velocity to decrease and consequently they sediment and simply roll on the bottom. The reduced gravity causes the slug to disintegrate and the center of mass of the slug moves upwards against gravity. The increased viscosity of the fluid, for a fixed pressure gradient, causes the particle to settle on the bottom of the channel under gravity.

APPROVAL PAGE

NUMERICAL STUDY OF PNEUMATIC CONVEYING OF POWDERS

Muhammad Mushahid Rafique Qureshi

Dr. Pushpendra Singh, Thesis Advisor — Date
Associate Professor of Mechanical Engineering, NJIT

Dr. Anthony D. Rosato, Thesis Co-Advisor — Date
Professor of Mechanical Engineering, NJIT

Dr. Ian S. Fischer, Committee Member — Date
Associate Professor of Mechanical Engineering, NJIT

BIOGRAPHICAL SKETCH

Author: Muhammad Mushahid Rafique Qureshi

Degree: Master of Science

Date: January 2003

Undergraduate and Graduate Education:

- Master of Science in Mechanical Engineering,
  New Jersey Institute of Technology, Newark, NJ, USA, 2003

- Bachelor of Engineering in Mechanical Engineering,
  University of Engineering and Technology, Lahore, Pakistan, 2000

Major: Mechanical Engineering

To my beloved parents,

ACKNOWLEDGEMENT

I would like to thank Almighty ALLAH first and then I would like to express my deepest appreciation to Dr. Pushpendra Singh who not only served as my research supervisor, providing valuable and countless resources, insight, and intuition, but also constantly gave me support, encouragement and reassurance. This work would have remained incomplete without his great interest as well as methodology. I would like to pay special thanks to Dr. Singh for putting in his time and efforts and encouraging me to achieve all that I have.

I would also like to extend my sincere gratitude to the members of my committee, Dr. Fischer and Dr. Rosato. I am particularly appreciative of their effort in reviewing my work on such short notice.

In the last, I would like to thank my family and friends for all their support.

TABLE OF CONTENTS

TABLE OF CONTENTS

Chapter **Page**

LIST OF FIGURES

LIST OF TABLES

Table **Page**

CHAPTER 1

INTRODUCTION

1.1 Objective

The objective of this thesis is to understand the dynamical behavior of the two-phase gas-solid flows, and to quantify the role of parameters that are important in the development and stability of the dense phase pneumatic transport by using the predictive capability available at New Jersey Institute of Technology. The current work entails an analytical/computational study of dense phase pneumatic transport with a focus on the role of gravity.

Quantitative comparisons between experimental data and numerical results for different parameter values will benchmark the simulations. The long term objective is to be able to obtain an accurate and quantitative assessment of the role of gravity in the transport of particulate materials so that gas-solid conveying systems can be developed for use in the extraterrestrial environments.

1.2 Motivation

The development of extraterrestrial environments will ultimately require the use of locally available raw materials. The capability to transport various natural planetary minerals and ores as well as process and handle other particulates will play a crucial role for mankind to establish colonies and settlements outside of Earth. In order to put this view into prospective, consider the situation of earth where the usage of granular materials spans a host of industries, such as agriculture, ceramics, chemicals, electronic, energy geological systems, manufacturing, minerals and ores, pharmaceuticals, plastics

pollution control systems and powder metallurgy. Each year, billions of tons of materials are handled and processed to produce the goods and services that are in everyday use. As an example the mining industry, where in the United States, 2.01×10^9 tons of crushed sand and gravel was mined for consumption during the first six months of 1999, in the United Kingdom, 165,600,000 tons of granular materials are produced each year, while the annual world production of coal is approximately 4.7×10^9. The above examples provide a glimpse of the potential magnitudes that may rise as mankind progress to create habitable environments beyond the confines of Earth.

Solid processing on earth involves essentially five basic operations: particle creation, size reduction, size enlargement, separation and mixing, which rely heavily on the ability to transport the particulate granular materials. On earth, conveying systems such as chutes, vibratory feeders and hoppers make use of gravity to assist in or cause the material flow, while pneumatic systems transport particles in a stream of gas through a pipeline network. In an extraterrestrial environment where there is only minimal or no gravity, pneumatic systems must be used.

1.3 Models For Pneumatic Transport

There are essentially two ways of pneumatically transporting granular materials.

1. Dilute Phase Conveying
2. Dense phase Conveying

1.3.1 Dilute Phase Conveying

It involves large gas flow rates that can cause particles to be entrained in and carried with the gas at high velocities. Over a period of time, collisions of particles with the sections of the pipeline (especially at bends and elbows) at these high velocities can result in an overall weakening and degradation of the conduit, thereby compromising its integrity. It is noticeable that the erosion of pipes and degradation of particles is proportional to the conveying velocity to 3^{rd} or 5^{th} power. Thus in a micro-gravity environment, safety issues become critical. In addition, the high velocities character of dilute phase systems can lead to particle attrition, a generally undesirable result. Consequently, a reduction in the amount of erosion of the pipeline and degradation or attrition of the flowing particles requires low velocities of transport. Another consideration is that the requisite high power consumption in dilute phase systems can also pose an obstacle in an extraterrestrial environment, despite the fact that relatively low pressures are needed.

1.3.2 Dense Phase Conveying

The integrity of the pipe can be greatly increased by the use of pulsed piston flows of particles, which is one mode of dense phase conveying. Here, the flow essentially consists of alternating plugs of densely packed particles and gas. Because this over-all strategy provides a mean to transport material at velocities of approximately 1m/s, problems associated with erosion of the pipeline and attrition are not significant. In addition, the fact that particles in the plugs are densely packed means that a significantly greater amount of materials can be transported over far greater distances than is possible in dilute phase conveying. Thus smaller pipe diameters can be utilized than for the dilute

phase flow where larger pipe diameters are required to convey an equal amount of material. In addition, smaller dust collection requirements are needed for dense phase piston flows. All of these advantages indicate that the use of dense phase pneumatic conveying has great potential for use in extraterrestrial environments with little or no gravity.

The key issues in dense phase pulsed piston format is the interaction of the particles with the wall, the drag force of the gas flowing through the plug and the frontal and back stress in the plug. Each Model must consider these issues. In order to form a stable plug, a stationary layer of material should be deposited on the bottom of the pipe. The plug then moves over this layer having material from the layer incorporated into the plug as well as deposited from the plug at the trailing edge of the plug.

1.4 Reduced Gravity Effect

As the gravity is diminished, the importance of the deposited layer is again subjected to question. For reduced gravity the difference between horizontal and vertical flows is less defined. This will mean that plugs behave similarly no matter what orientation is present.

1.5 Existing Analytical Models of Dense Phase Conveying

A part of the task in the dense phase conveying is the prediction of the ability of the material to be conveyed. The other part of the task is to obtain reliable models that can provide the designer with overall energy requirements for the design. Results show that the models based on the work of Konard et al. (1980) are the most reliable to date.

The analysis based on the work of Konard et al. (1980) is described for cohesionless materials which includes a force balance and the classical Ergun equation for the flow of a gas through packed bed. Two types of failure of the plug were considered in this analysis; passive failure when the radial stress is greater than the axial stress (a pulling), and the active failure when the axial stress is greater than the radial stress (a pushing). By combining the two equations, the plug velocity was found. Konard assumed that the stress at the front and back of the plugs were the same. For plastic pellets the plugs were found to behave as passive units. Data taken by the Jenike shear cell device can be employed directly into Konard equation to determine the pressure loss across the plug, i.e., wall cohesion, angle of wall friction, particle shear, the angle of internal friction and the stress transmission coefficient.

Ergun developed an empirical expression for the pressure loss across a packed bed for both the laminar and turbulent gas flow regimes. Ergun's expression can be considered as for a moving packed bed to obtain an expression for the pressure loss.

Muschelknautz (1969) carried out a comprehensive study on the pneumatic conveying and developed a model for dense phase conveying that considered the pressure needed to move the plug to be proportional to the frictional force required to move the plug in the pipeline. Employing the gas law expression, he obtained an exponential expression for the pressure loss over a plug with distance. In application of his model, he employed the entire system pressure loss without knowledge of the detailed condition inside the pipeline. Assumptions concerning the particle-wall friction are essential in employing this model.

Later, Aziz and Klinzing (1988) modified the Muschelknautz expression as reported by Weber (1973) including the shear stress developed by Konard. These researchers also probed a modification of the Konard model for particles with cohesion present. It was clear from this analysis of fine particles with cohesion that the manner in which the plugs were formed was crucial for developing a correct model. Some of their findings showed as exponential pressure loss with the distance while others were linear with plug length. The differences in these findings can be likened to the work of Dickson et al. (1978). These investigators found that by forming impermeable plugs that were dragged through the pipe, an exponential behavior of pressure loss with distance was seen. When the plug experienced some permeation of gas and a solid plug was not employed, a linear behavior for the same parameters was observed. This behavior is also seen in a simple apparatus devised by Arnold (1997) where a small amount of fluidization gas through a plug greatly reduces the forces necessary to convey the plug.

The previous analysis considered the topic of plug flow motion in a rather simplified fashion. These idealized plug behaviors are seen in experiments. The deposition of the material on the bottom of the pipeline in horizontal flow often occurs. To address this situation Mi, under the direction of Wypch (1985), used the Konard development with some modifications and assumptions. They treated the whole pipeline in the analysis of the pressure loss and used a different expression than Konard for the frontal stress on the plug. In this model, it was also assumed that the particle velocity in the plug was the same as the mean plug velocity.

In an attempt to consider the proper friction representation for the material and the wall, Kano et al. (1984) developed an expression that had a general exponential pressure increase with distance along the plug. The experiments were carried out on fine 16μm diameter calcium carbonate powder. The results followed the data well but presented difficulty in representing the plug flows of larger granular materials.

1.6 Computational Approaches in Gas-Solid Flows

The three common computational approaches for modeling of gas-solid flows are;

1. Continuum Method
2. Discrete Element Method (DEM)
3. Direct Numerical Simulation (DNS)

1.6.1 Continuum Method

This approach is computationally least demanding and therefore, at least partially for this reason, has been used extensively in the past. However, since it resolves flow at the coarsest scale (scales much larger than the size of particles), it cannot be easily used for understanding the phenomena that are controlled by the particle-particle and gas-particle interactions, e.g. formation of slugs.

1.6.2 Discrete Element Method (DEM)

This approach resolves the flow at the intermediate scales requiring models for the gas-particle and particle-particle interactions. This technique also has been only partly

successful as the models for interaction between the phases are approximate and thus may not correctly include particle scale features.

1.6.3 Direct Numerical Simulation (DNS)

This approach, which has become viable only in the past few years, is computationally most demanding, as it resolves flow at the finest scales. This powerful methodology simulates dynamics at scales much smaller than the size of particles, and thus could be used to understand previously unexplained phenomena such as formation of plugs in gas-solid flows. Such calculations represent a powerful and essential approach to modeling and simulation of industrial scale gas-solid flow problems.

CHAPTER 2

MODELLING APPROACHES

2.1 Continuum Approach

As discussed below, when the continuum approach works, it is the most efficient and practical approach for describing the macro-scale dynamics of gas-solid flows in industrial scale devices, e.g., the gas-solid flow in a conduit. The governing continuum equations are obtained by ensemble or volume averaging the point equations of motion for the particles and the gas described above. In order to obtain these equations, one must make several approximations, and for this reason several slightly different forms have been proposed in the literature. For example, one of the popular forms of these equations is:

$$\frac{\partial}{\partial t}\left(\rho_f \varepsilon_f\right)+\nabla.(\rho_f \varepsilon_f \mathbf{u}_f)=0$$

$$\frac{\partial}{\partial t}\left(\rho_p (1-\varepsilon_f)\right)+\nabla.(\rho_p (1-\varepsilon_f)\mathbf{u}_p)=0$$

$$\rho_f \varepsilon_f\left[\frac{\partial}{\partial t}\mathbf{u}_f+\mathbf{u}_f.\nabla\mathbf{u}_f\right]=\varepsilon_f \nabla.\mathbf{E}_f-\varepsilon_f \mathbf{F}+\varepsilon_f \rho_f \mathbf{g}$$

$$\rho_p (1-\varepsilon_f)\left[\frac{\partial}{\partial t}\mathbf{u}_p+\mathbf{u}_p.\nabla\mathbf{u}_p\right]=(1-\varepsilon_f)\nabla.\mathbf{E}_f+\varepsilon_f \mathbf{F}+(1-\varepsilon_f)\rho_s \mathbf{g}+\nabla\cdot\mathbf{E}_s$$

Here, ε_f and ε_p are the fluid and particle phase volume fractions, $\mathbf{u}_f$ and $\mathbf{u}_p$ are the fluid and particle phase velocities, ρ_f and ρ_p are the fluid and particle phase densities, $\mathbf{F}$ is the local average force exerted by the gas on the particles, $\mathbf{E}_f$ is the local average stress tensor for the gas, $\mathbf{E}_p$ is the local average stress tensor for the particle phase and $\mathbf{g}$ is the acceleration due to gravity. Notice that the above system of equations is not closed, as the functional forms of $\mathbf{E}_f$, $\mathbf{E}_p$ and $\mathbf{F}$ are not known.

In this approach, the particle-scale features that are related to the flow patterns at the particle scale are not resolved, but their effects are included in the averaged continuum equations. At present, the exact functional forms of the relations that are needed to close these systems of equations are not known. However, several ad hoc relations have been proposed to close the system of equations that have had limited success. For example, the stress tensor E_p for the particle phase in component form is given by,

$$E_{pik} = -p_p \delta_{ik} + \lambda_p(\varepsilon_f)\frac{\partial \mathbf{u}_{pm}}{\partial x_m}\delta_{ik} + \mu_p(\varepsilon_f)\left[\frac{\partial \mathbf{u}_{pi}}{\partial x_k} + \frac{\partial \mathbf{u}_{pk}}{\partial x_i} - \frac{2}{3}\delta_{ik}\frac{\partial \mathbf{u}_{pm}}{\partial x_m}\right]$$

where $\mathbf{u}_p$ is the particle phase velocity, μ_p is viscosity, λ_p is bulk viscosity and p_p is the particle phase pressure. It is noteworthy that in this approach both the solid and gas phases are considered continuous, and thus there are no moving boundaries. The governing equations thus can be solved using a spatially fixed grid. In fact, it is the only viable approach for many practical applications, as in most gas-solid systems there are trillions of particles and therefore it is simply not practical to solve for the trajectory of each one of them.

2.2 Discrete Element Method

At the next finer level is the Discrete Element Method (DEM). In this approach, the particles are followed in time along their trajectories through the flow field. At every given time step, the new positions of the particles and the new translational and rotational velocities are calculated according to the forces (collisional interactions, drag force, gravitational force, lift forces due to shear and particle rotation) acting on them. This

method, an outgrowth of molecular dynamics simulations, used in statistical physics Alder (1956) and Ashurst (1973), and independently developed by Cundall (1974), has been used successfully to study the single-phase flow of granular materials under a variety of conditions. See for example Walton (1992), Rosato et al. (1994) and Rosato et al. (1995).

In the absence of an interstitial fluid phase, two types of particle collision models are commonly used in DEM simulations, i.e., either hard or soft binary interactions. For hard particles, the post-collisional kinematics (positions and velocities of the particles) are determined by their pre-collisional values and three material-dependent parameters: (e, β, μ), which are the normal and rotational restitution coefficients and the friction coefficient, respectively. See for example Lubachevsky (1991) and Dippel (1995). Because collisions are "instantaneous" using hard particle models, flows in which continuous contacts occur could be problematic. On the other hand, soft interactions admit transmitted forces that are functions of an allowed small overlap (i.e., generally less than approximately 1% of the particle size) between the colliding particles. Thus, the resulting finite contact duration eliminates potential problems imposed by hard particle models.

The soft sphere interactions developed by Walton et al. (1986) and Walton et al. (1991) are popularly used. Here, the normal force, (i.e., in the direction along the line of centers of the contacting spheres), is determined by loading and unloading springs of stiffness K_1 and K_2, respectively. Thus,

$$F_n = \begin{cases} K_1 \alpha^{\square}, & \text{for loading} \\ K_2 (\alpha - \alpha_o)^{\beta}, & \text{for unloading} \end{cases}$$

where α_o is the overlap remaining when $F_n = 0$. The loading path for the linear case (β = 1) is illustrated in Figure 2.1. Loading is along path *AB*, and if unloading occurs at *B*, it follows the line *BC* to α_o. At this point, if there is no reloading (which would follow *CBD* with unloading along *DFCA)*, particles continue to separate at constant velocity to a zero overlap. The linear model produces a constant restitution coefficient given by $e = \sqrt{K_1/K_2}$ if the unloading paths (lines *BC* and *DF* in Figure 2.1) have the same slope K_2. A variable restitution coefficient as a function of the relative approach velocity v_o may be obtained by allowing K_2 to be linearly dependent on the maximum force realized before unloading $K_2 = K_1 + cF_m$. This is given by $e = \sqrt{\Omega_o / (cv_o + \Omega_o)}$, where the parameter c is empirically determined and $\Omega_o \equiv \sqrt{2K_1/m}$. It should be noted that models yielding the theoretically predicted behavior $e \propto v_o^{-1/4}$ Johnson (1987) (i.e., plastic deformation in the contact region) have been developed which capture the rebound of particles from surfaces after elastic-plastic impact has occurred.

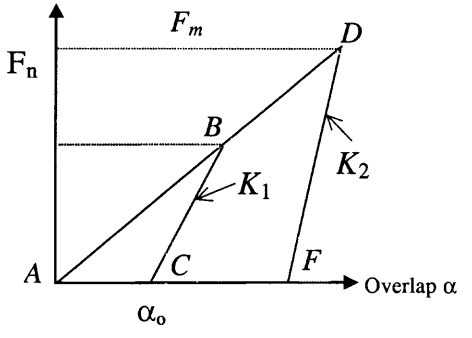

Figure 2.1 Normal Force Model of Walton and Braun

In the tangential direction, Walton (1986) approximated the theory of Mindlin (1953) for elastic spheres subjected to tangential loading, resulting in a one-dimensional "incrementally slipping" friction force model for disks which was subsequently extended to three dimensions for spheres (Walton 1986). Although this does not include the effects of contacts that experience rotation coupled with tangential sliding, particles can rotate due to the transmission of tangential impulse. In accordance with the theory, full sliding of the contact occurs when the limiting force μF_n is attained as a result of increasing elastic strain. This takes place when the contact tangential stiffness

$$K_{\tan} = \begin{cases} K_0[1-(T-T^*)/(\mu F_n - T^*)]^{1/3}, T \text{ increasing} \\ K_0[1-(T^*-T)/(\mu F_n + T^*)]^{1/3}, T \text{ decreasing} \end{cases}$$

decreases to zero. In the latter expression, F_n and T are the magnitudes of the current normal and tangential forces, respectively, $K_0 \approx 0.8K_1$ is an initial tangential stiffness, μ is the friction coefficient and T^* is the turning point value of T. While it is remarked that more "accurate" models do exist (see for example Vu-Quoc (1999)), the added complexity here may be unnecessary because of the intention to incorporate the gas phase into the code.

2.3 Direct Numerical Simulation Method

In the DNS approach, the detailed motion of both gas and particles, at scales smaller than the size of particles, is resolved by numerically solving the exact initial value problem for the gas-particle system (within discretization errors). The popularity of this approach is rooted in the fact that the information contained in the equations of motion can be extracted without any approximation using direct numerical simulations (see Hu (1996),

Hu (1998), Joseph (1998) and Tezduyar (1992)). This involves simultaneous integration of the governing equations for both continuous (gas) and discontinuous (particle) phases. Singh and his KDI collaborators have recently developed a distributed Lagrange multiplier/fictitious domain method (DLM), which allows to efficiently simulate the motion of thousands of particles suspended in a Newtonian fluid at finite Reynolds number, Re ~O(1000) (see Singh et al. (2000), Singh et al. (2001), Glowinski et al. (1997), Patankar et al. (2001) and Glowinski et al. (1998)). Here it is noted that in Brady et al. (1988), the DNS approach for Stokes fluids was developed, while in Hu et al. (1996), an approach based on an arbitrary Eulerian-Lagrangian method was developed for the Navier-Stokes equations.

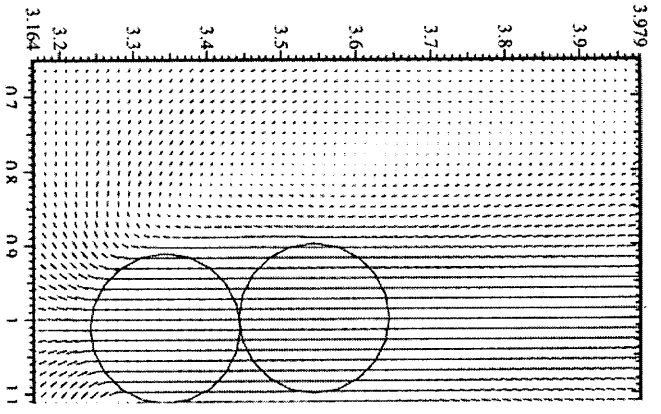

Figure 2.2 The velocity distribution inside and outside the particle is shown. The DLM method is used to force the velocity field inside a particle to be that of a rigid body.

The ability of the code to accurately capture the interaction of the particles with a gas is demonstrated in the recent study of air entrainment effects on the flow of powders Singh et al. (1999). The direct numerical simulations showed that the aerodynamic forces are important in determining the flow properties of powders when the particles size is of

the order of 1000 μm or smaller. Specifically, when a granular system slides downwards inside a closed channel inclined at 60° to the horizontal the particles on the surface are lifted away by the aerodynamic forces which causes a partial blockage of the channel. The back flow of the air is hindered and an adverse pressure gradient develops in the channel that decelerates the downward motion of the powder. The adverse pressure gradient, in fact, is so strong that the magnitude of downward velocity of the center of mass decreases during the time interval for which the channel is partially blocked. Also when all particles were of the same density, the aerodynamic forces enhanced mixing. On the other hand, in a mixture containing particles of two different densities, the aerodynamic forces resulted in segregation.

One of the key features of the DLM method is that the gas-particle system is treated implicitly by using a combined weak formulation where the forces and moments between the particles and gas cancel, as they are internal to the combined system. In this combined weak formulation, gas flow equations are solved everywhere in the domain, including inside the particles. The flow inside the particles is forced to be a rigid body motion using the distributed Lagrange multiplier method (see Figure 2.2). The Marchuk-Yanenko operator-splitting technique (Section 4.6) is used to decouple the difficulties associated with the incompressibility constraint, the nonlinear convection term, and the rigid body motion constraint. This gives rise to the three sub-problems that are solved using matrix-free fast algorithms.

2.4 Present Numerical Modeling Approach

The DLM code is employed to study the motion of several of particles in periodic domains, with linear dimension two or more times larger than that of the plug, subjected to pressure gradient and gravitational body forces. These numerical results are used for understanding the particle-scale mechanisms that are important in the formation of plug, as well as in the accumulation of particles in the front of the plug and the attrition of the particles at its back. The results of these calculations can be used to model the inter-phase interaction force and stresses in the averaged equations of motion, as well as for validating and improving macroscopic models for the plugs.

The particle-particle interactions in both DEM and DLM approaches are simulated using the so-called collision models. The velocities after collision of the particles emerging from sliding and non-sliding collisions are calculated by considering the balance of linear and angular momenta in the collisions and the coefficients of restitution and sliding friction. In order to optimize the code with respect to searching for collision partners, the simulated domain is sectioned into smaller cells and only the particles that are found in either the same or neighboring cells are examined for collisions. All relevant flow information for the particle phase can be extracted from the simulations via long-time averaging. Realistic collision models are already available in DEM code as described in Section 2.2

CHAPTER 3

LITERATURE REVIEW

3.1 Pneumatic Conveying

Great improvements are continuously being made in the solid freeform fabrication (SFF) industry in terms of processes and materials. The use of fine powders as its build material provides the potential for the Selective Laser Sintering (SLS), Three-Dimensional Printing (3DP), and Freeform Powder Molding (FPM) processes to be altered to create continuously heterogeneous material composition (Fitzgerald 1996).

The flow of powders represents a greater challenge than that of the low viscosity binder and printing ink. Geldart (1990) states that powders are not solids, although they can withstand some deformation. Powders are not liquid, although they can be made to flow. Powders are not gases, although they can be compressed. The space between particles is filled with gases and therefore the solid/gas interaction, the interparticle contact area, and adhesion between particles must be considered during flow analysis.

In the past, solids were commonly transported in suspension form via lean-phase conveying. Lean-phase conveying uses a low volumetric concentration of solids, typically less than ten percent. Conveying in this form may cause a few problems. There is a high rate of pipe wear and particle attrition due to the high velocities. Depositing powder in this manner for use in SLS, 3DP, or FPM would also have several other undesired effects. For instance, it is likely to deposit the powder with too large force and disturb the underlying powder bed, and the control over the accuracy of desired powder compositions may be lost due to the local sandstorm effect.

An alternate transportation approach is dense-phase conveying. It is defined as the conveying of particles by air along a pipe that is filled with particles at one or more cross-sections (Konrad 1986). It offers improvements in slower air speeds and lower volumes of gas required for transporting the same amount of material, which is of particular importance if an inert gas is needed to reduce the risk of explosions (Konrad 1986).

Albright et al. (1951) was one of the first to study dense-phase conveying. His goal was to minimize the amount of gas required to feed solids into a coal gasification reactor. Since then, its use has grown substantially.

Dense-phase conveying appears more appropriate for powder deposition in SLS, 3DP, and FPM. The slower air speeds are less likely to disturb the previously deposited powder bed and greater control over powder placement could be gained. The lower volumes of air should also benefit the SLS process that uses an inert gas, usually nitrogen, in the process chamber to prevent oxidation or explosions (Behrendt et al. 1995).

In dense-phase conveying, since a section of the pipeline is completely filled with material, clogging can be a common occurrence and the flow somewhat unstable. One approach to reduce this clogging is to artificially create distinct plugs of material. Conveying in this form is known as plug-phase conveying.

Konrad reports of three commercial systems developed to deal exclusively with plug-phase conveying. In the first, a bypass system was developed by Lippert (1966) to stabilize pressure fluctuations in plug-phase conveying (Figure 3.1). The conveying pipeline has an additional bypass pipeline with holes at set intervals. No additional air is

blown into this bypass pipe. It merely serves as an alternative route for the conveying air to break up lengthy plugs.

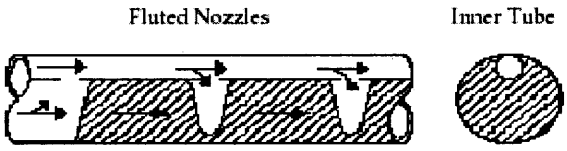

Figure 3.1 Internal secondary air pipe system (Lippert 1966).

The other two systems artificially induce plugs of solid material separated by plugs of air, which is effected by the addition of a secondary air source. There are distinct plugs of material separated by plugs of air. One such system uses an air knife to provide regular pulses of air that will chop up the moving solids fed into the pipeline (Figure 3.2) (Geldart 1990). In the other system, the plugs are created by using alternating air valves (Figure 3.3) (Geldart 1990).

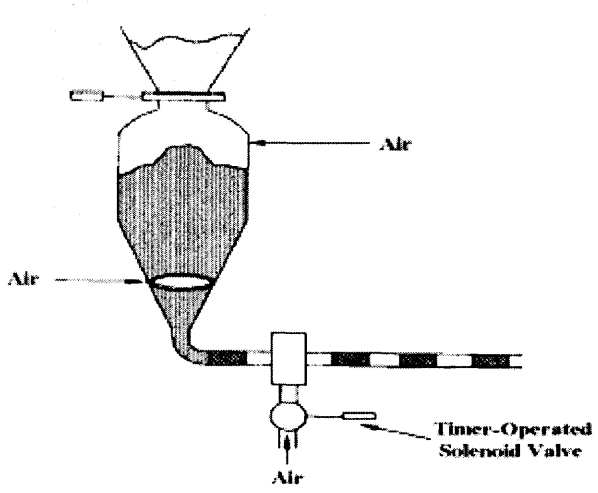

Figure 3.2 Plug formation using timer operated air knife. (Geldart 1990)

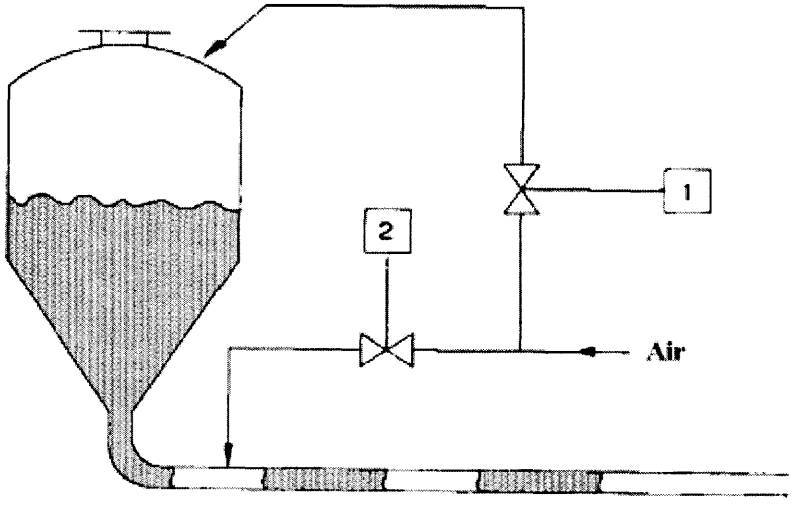

Figure 3.3 Plug formation using alternating air valves. (Geldart 1990)

Powder delivery systems similar to the commercial plug-phase conveying systems, utilizing an additional air source, with some modifications can be used for SLS, FPM and 3DP. These systems do not provide a continuous flow of powder, but this can be overcome by running two parallel pipelines operating at opposite phases i.e., when there is a discharge of powder through one nozzle, the other nozzle will discharge the air and vice versa (Fitzgerald 1996). They would also require the addition of a dispensing nozzle to mix and to accurately deposit the powder onto the underlying powder bed. Various powders must be delivered to the dispensing nozzle through different tubing systems for continuously heterogeneous material deposition. By controlling the velocity of plugs throughout each of the material supply systems, different proportions of each material could be combined and deposited.

3.1.1 Pressure Drop Across Industrial Plug

Experimental evidence available in literature regarding plug-phase conveying is contradictory. Lippert (1966) measured the pressure drop across individual moving plugs in a horizontal pipeline. The pressure drop was found to be proportional to the square of plug length divided by the pipe diameter. Flain (1972) used a fine cohesive material to construct plugs of a given length in a horizontal pipeline. He measured the pressure drop required to move these plugs and concluded that this pressure drop was proportional to the square of the plug length. Dickson et al. (1978), however, suggest a linear relationship for both coarse and fine materials (Fine powders are defined as those with particle sizes between 1 and 100 μm. (Brown et al. 1970))

Konrad (1986) has done extensive work on plug-phase pneumatic conveying. He found that solid materials flow in discrete plugs that fill the tube cross-section at approximately maximum packing density. Between the plugs, the upper part of the pipe contains moving air with some dispersed particles. The lower half is filled with a stationary bed of particles (Figure 3.4). Each plug picks up the particle bed in front of it, while leaving behind a stationary layer of nearly equal thickness behind it.

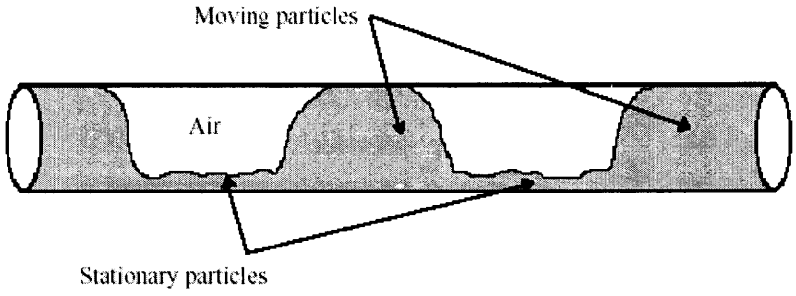

Figure 3.4 Flow pattern of plug-phase conveying.

Konrad et al. (1980) developed a theoretical model to predict the pipeline pressure drop in horizontal dense-phase plug conveying. The theory is based on the following premises. The material is conveyed only in the plugs and in the regions just in front of and behind them. There is a layer of stationary material between the plugs. The flow pattern resembles that of a gas-liquid system. The pressure drop required to move a single horizontal plug is therefore given by the expression:

$$\frac{\Delta P}{H} = 2\rho_B\mu_w + \frac{4\mu_w k_w F}{D} + \frac{4\mu_w(k_w+1)C.\cos\phi\cos(\omega+\varphi_w)}{D} + \frac{4C_w}{D}$$

Where,

H = the plug length.

g = the acceleration due to gravity.

ϕ_w = the angle of wall friction.

k_w = the Jansen coefficient at the wall.

F = the stress on the front end of the plug.

$\omega = \sin^{-1} (\sin \phi_w / \sin \phi)$.

ρ_B = the bulk density.

$\mu_w = \tan \phi_w$.

ϕ = the angle of internal friction.

D = the pipe diameter.

C = the interparticle cohesion.

C_w = the particle wall cohesion.

This equation can only be used to predict general flow trends in the experimental apparatus since it uses multiple tubing systems with several of the above parameters being unknown. There is, therefore, a need to collect experimental data for each of these tubing systems in order to determine these parameters and thereby enable the use of this equation.

3.2 Models for Gas-Solid flows in Horizontal Dense Phase Pneumatic Conveying

Konard (1986) predicted the air-pressure profile within a long dense phase pneumatic conveying pipeline. Through his experiments, he showed that the pressure gradient decreases in magnitude as the air expands down the pipeline. He also proved that this expansion is isothermal rather that adiabatic. He integrated the pressure gradient to predict the pressure drop along the pipeline numerically and compared the results of pressure profile obtained with published experimental data for the transport of sand. The pressure profiles obtained entirely from the theory of Konard et al. (1980) consistently under predict those of the data pressure drops observed for sand which he explained to be due to unavailability of many parameters for sand.

Klinzing et al. (1990) proposed the dense phase pneumatic conveying as a potential method to deliver the fine coal from hopper into boiler since it requires a low amount of transport gas. They discussed the operational characteristics, flow patterns and pressure loss behavior for the plug flow conveying of fine cohesive coals. They also presented two pressure drop equations (one for each full-plug and half-plug form conveying) to predict the pressure drop across the plug for the plug lengths. The results of their models were in agreement within ± 20% of the experimental data, showing the reliability of these models as basis for future investigations.

Hong et al. (1993) developed the model for gas-solid stratified flow based on the assumption that pressure in a sliding bed obeys a hydrostatic pressure distribution. In addition to that, they added the effects of saltation and sliding of suspended particles at the surface of the sliding bed. The predicted pressure drop from the developed model coincides within ± 30% with the experimental data for conveying medium size sand and fine lime in an 8 m long pipe with a diameter of 20 mm under a wide rang of solids loading from 30 to 200. The model was developed to understand the interaction mechanism between the suspension and sliding bed with high solid/gas mass flow rate ratio (solids loading). Based on this model, the dense phase regions of Zenz-type phase diagrams (i.e., the plot of pressure drop versus superficial gas velocity, with solids mass flow rate and solids loading as parameters) have been quite reasonably predicted for the horizontal pneumatic transport of particles. (Hong et al. 1995)

McKee et al. (1995) used the non-invasive Electrical Capacitance Tomographic (ECT) technique to monitor the behavior of industrial scale pneumatic conveyors. Plug like flow regimes were recorded by the instrument, for dense phase conveying, showing a

slug of solids moving ahead of a settled layer of particles on the pipe base making an overall effect being that of wave-like motion. The slug entrains particles in its path and accelerates them in mixing zone to a velocity that has the same order of magnitude as the average particle velocity over the entire pipe cross section. The slug celerity (wave velocity) is larger than the average particle velocity. Particles are shed from the back of the slug to a trailing layer and after traveling a short distance cease to move. They concluded that as the mass flow rate of solids increases, the area of a settled layer decreases while the average particle velocity also increases.

Wypych et al. (1997) presented a new test-design procedure that can be used to predict the pressure drop and slug velocity, accurately in large-scale systems, in low-velocity slug flows regardless of the particle shape (regular or irregular). They based their model on particle properties and data from a simple vertical test chamber. This procedure can be applied to bulk solids materials with regular, irregular and/or unusual physical properties (e.g., different shape, density, size and size distribution), as long as dense phase pneumatic conveying mode is applicable. Their technique was even able to predict well the pressure gradient for the pneumatic conveying of pet food (very large and irregular shape particles).

Carpinlioglu et al. (1997) used an experimental approach to find the development length, in the particulate flows, which was treated as the necessary distance downstream of the particle feeder for the attainment of homogenous particle distribution in air. It was estimated by evaluating the variation of local friction factors, f_{p+a} , calculated from the measurements of local static pressure gradients, dp/dx. The measurements were conducted in airflow, based on mean air velocity and pipe inner diameter, in the range

$51000 \leq Re \leq 109000$ at particle loading ratios of 5% to 30% to determine the influence of Re and particle loading ratios on the development length. They concluded that the development length of two-phase particulate flow is a strong function of Re.

Mason et al. (1998) worked on the main problem encountered while designing, optimizing and updating the conveying systems, which is the determination of the air supply necessary to achieve a particular duty (solid mass flow rate). Many correlations exist to predict the pressure drop necessary to drive the flow, and gas velocities necessary for successful operation. The design methods, which incorporate these correlations, are limited in their flexibility. They developed the simulations so that the flexibility of the design method can be increased as well as more than one correlation can be employed. The algorithm designed, allows a variety of design criteria of a pneumatic conveying system to be simulated.

Mason and Levy (1998) performed a through study on the effect of a bend on the distribution of particles in a pipe cross-section and segregation in pneumatic conveying systems. They solved the finite-volume equations for mass conservation and momentum conservation of two phases. They found that the cross sectional concentration of the particles a few meters after the bend is not uniform and that the particles tend to concentrate around the pipe wall. They concluded that the path taken by the particles after the bend is strongly dependent upon their sizes. Since a real particulate phase (i.e., powder, granular material, etc.) is composed of particles with a range of different sizes, this would lead to segregation of the particles in the pipe section following a bend.

Taylor (1998) proposed that the selection and design of pneumatic conveying involve key considerations of energy consumption and effects upon the product.

Pneumatic conveying must compete the other methods such as mechanical and hydraulic conveying in terms of capital and operating costs and in ability to operate with minimal effects upon the environment and the particles. He measured the specific energy and particle attrition for dense phase pneumatic conveying, being one of the best options for above purpose, for a limited range of particulate. The results were compared with published correlations and the implications discussed for energy consumption, particle and bulk properties. Specific energy consumption correlated best with solid/air mass ratio but particle attrition was very low due to relatively low conveying velocity involved.

Luke et al. (1999) proposed that the detailed knowledge of the flow regimes and a number of flow properties is essential in the investigation and control of flow phenomenon in the pneumatic conveying of solids. Electrical capacitance tomography (ECT) was described as a powerful tool for this purpose, especially for the dense phase plug flow. They applied ECT to dense phase powder conveying in an experimental vacuum system for the visualization of plug size, shape and velocity. They analyzed the measured gas and solid flow rates in an attempt to ultimately provide a basis for comprehensive on-line analysis. A number of statistical estimators were selected and used in data processing to distinguish between particular types of dense phase flow. This method could be used for on-line control of dense phase pneumatic conveyors.

Neuffer et al. (1999) presented the ECT to visualize solid movement within conveying pipelines and suggested that this technique, in addition to being durable, cheap and potentially effective, can be used as primary sensory input to an optimal control system. They designed and constructed a pneumatic conveying rig in order to simulate the slug flow of plastic pellets using air as a transportation media. After analyzing the

flow, they described two parallel control strategies in association with an ECT system for the optimization of pneumatic conveyors. One technique utilizes the parametric modeling of conveying systems, while the other is based on a fuzzy logic approach.

Levy (2000) used the two fluid theory in order to model plug flow in horizontal pneumatic conveying. He developed a three dimensional model which enabled the simulation of the dense phase flow. A finite volume numerical method was used to solve the conservation equation of mass and momentum. He also introduced the solids contact stress and described it as a function of bulk density. The numerical simulation demonstrated the formation and deformation of plugs along a horizontal pipe. Both the axial and radial pressure drops were examined. He concluded that due to plug creation and destruction, it is impossible to obtain the plug velocity by cross-correlation between various radial or axial pressure drops. The change of the radial pressure drop is a very typical property of plug flow and as a result can be used to identify the transition from dilute phase to dense phase flow. Furthermore, the operational condition of pneumatic conveying system can be examined by this flow property.

Matsuda et al. (2000) experimentally observed the flow characteristics of powder (i.e., passing period, velocity and length of dune and plug and pressure drop in the pipeline) with variation of the pipe diameter, inclination of the pipe, pump revolution, powder mass flow rate and air velocity. In the design and practical use, it is very important to know the pressure drop due to powder that is why the relation between the coefficient of the additional pressure drop due to powder and Froude number is clarified.

Mason et al. (2001) developed a new model for non-suspension moving-bed type of flow in horizontal pipes where the flow is modeled as two layers i.e., a dilute gas-

solids mixture flowing above a dense gas-solids mixture. For each layer, the conservation equations for mass, momentum and energy were solved for both the gas and solid phases. In addition, mass, momentum and energy transfers between the two layers were incorporated in the model. A single pressure was shared between the two layers. Other phenomena (such as the momentum transfer between the gas and solid layer) were described by the sub-models. All this resulted in a model that behaved in a similar manner to experimental observations. The pressure profile and the depth of dense layer, predicted by the model, show reasonable agreement with the experimental observations.

Sundaresan (2001), in his attempt to explore some outstanding issues in the handling of cohesionless particles, presented the difficulties in modeling the dense phase pneumatic conveying. He suggested that the greater challenge is to specify, in a reliable manner, the closure relations (for the effective stresses and the interphase interaction) in terms of gas and particle properties. In particular, low velocity slug flow can be achieved as one of the regimes (see Figure 3.5) where particle damage can be minimized.

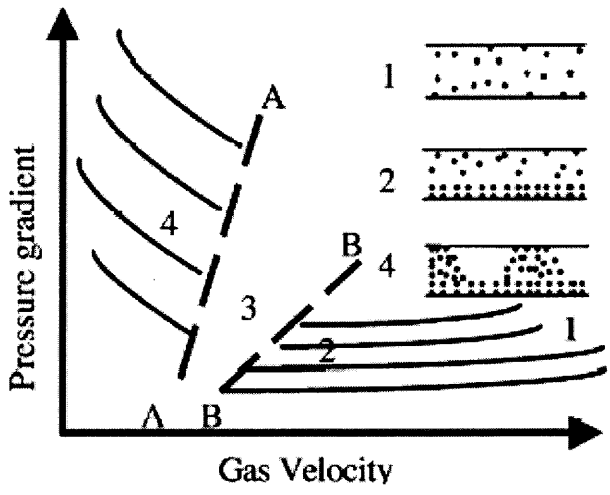

Figure 3.5 Schematic representations of pneumatic conveying characteristics for granular particles. 1 Dilute phase transport; 2 conveying in layers; 3 unstable one; 4 slug flow. Solid lines show lines of constant solids flux. The broken lines demarcate the regime of unstable operation. AA—dense-phase slugging boundary; BB—dilute phase boundary. (Sundaresan 2001)

One of the prominent features seen in Figure 3.5 is that at the intermediate conditions, unstable transport regimes are obtained where flow occurs with very large increase in gas pressure and the stresses exerted on the duct by the moving slugs. The flow fluctuates from fast moving unstable slugs to dilute phase transport with increasing levels of deposition. The domination of any of the two modes depends on the location of the operating condition inside the unstable regime. The unstable slugs are dominant near the dense-phase slugging boundary, while they are infrequent near the dilute phase boundary. To predict the two boundaries of the unstable region for specified gas, particles and duct is also a challenge. In order to identify the instability and the stability

boundaries, one must understand how the particles inside the slug move and transmit stresses to the wall.

Klausner et al. (2002) recently proposed the fluid mechanics approach to describe the behavior of pneumatically conveyed powder plugs. They carried out experiments for horizontal flow of cohesive silica and kaolin powders over a range of gas superficial velocities and plug lengths. They observed a linear increase in pressure drop with plug length and nonlinear increase in pressure drop with increasing superficial velocity. They developed a two-layer model to predict the behavior in which the inner core was treated as a Coulomb solid and the shear region of the plug was treated as a frictional fluid. Powder rheology for cohesive and non-cohesive powders were measured, compared and found in agreement with the values predicted by the model.

In the past two decades, several researchers have tried to model the two-phase gas/solids flows. The emphasize being more on the experimental study rather than numerical study. However, analytically solving the flow mechanism at the finest scales is critically important in the design and optimization of the pneumatic conveying systems and to better understand the flow mechanism. In most of the industrial applications of the dense phase pneumatic conveying, the common problem may be the clogging of the channel as the flow develops. This study is done to explore the role of parameters that govern the development and stability of slug for a dense phase conveying with a focus on the role of gravity.

CHAPTER 4

GOVERNING EQUATIONS

4.1 Problem Statement and Numerical Method

The fluid is assumed to be Newtonian. In the simulations, it is assumed that the lubrication forces are large enough to prevent the particles from touching each other or the walls. This is enforced by applying a body force to the particles when the distance between two particles, or between a particle and a wall, is of the order of the element size.

Now, let us denote the domain containing the viscoelastic fluid and N particles by Ω, and the interior of the ith particle by $P_i(t)$. For simplicity, it is assumed that the domain is rectangular with boundary Γ. The four sides of the domain will be denoted by Γ_1, Γ_2, Γ_3, and Γ_4 (see Figure 4.1).

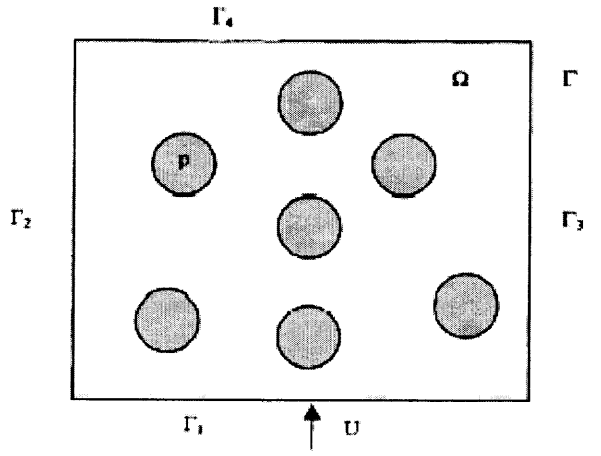

Figure 4.1 A typical rectangular domain used in our simulations.

The governing equations for the fluid-particle system are,

$$\rho_L\left[\frac{\partial \mathbf{u}}{\partial t}+\mathbf{u}.\nabla\mathbf{u}\right] = \rho_L g - \nabla p + \nabla.(2\eta D) \qquad \text{in } \Omega\backslash\overline{P(t)} \qquad (1)$$

$$\nabla\cdot\mathbf{u} = 0 \qquad \text{in } \Omega\backslash\overline{P(t)} \qquad (2)$$

$$\mathbf{u} = \mathbf{u}_L \qquad \text{on } \Gamma \qquad (3)$$

$$\mathbf{u} = \mathbf{U}_i + \omega_i \times \mathbf{r}_i \qquad \text{on } \partial P_i(t),\ i=1,\ldots,N, \qquad (4)$$

Here $\mathbf{u}$ is the velocity, p is the pressure, η is the viscosity, ρ_L is the density, D is the symmetric part of the velocity gradient tensor. The above equations are solved with the following initial conditions:

$$\mathbf{u}|_{t=0} = \mathbf{u}_0 \qquad (5)$$

where $\mathbf{u}_0$ is the known initial values of the velocity.

The particle velocity $\mathbf{U}_i$ and angular velocity ω_i are governed by

$$M_i\frac{d\mathbf{U}_i}{dt} = M_i\mathbf{g} + \mathbf{F}_i \qquad (6)$$

$$I_i\frac{d\omega_i}{dt} = T_i \qquad (7)$$

$$\mathbf{U}_i|_{t=0} = \mathbf{U}_{i,0} \qquad (8)$$

$$\omega_i |_{t=0} = \omega_{i,0} \tag{9}$$

where M_i and I_i are the mass and moment of inertia of the ith particle, and $\mathbf{F}_i$ and $\mathbf{T}_i$ are the force and torque acting on the ith particle. In this investigation it is assumed that the particles are circular, and therefore there is no need to keep track of the particle orientation. The particle positions are obtained from

$$\frac{d\mathbf{X}_i}{dt} = \mathbf{U}_i \tag{10}$$

$$\mathbf{X}_i |_{t=0} = \mathbf{X}_{i,0} \tag{11}$$

where

$X_{i,0}$ is the position of the ith particle at time t=0.

4.2 Collision Strategy

The collisions among the particles, and the particles and the domain walls, are prevented by applying a body force that acts when the distance between two particles, or between a particle and a wall, is of the order of the element size. This additional body force,which is repulsive in nature, is added to equation (8). The particle-particle repulsive force is given by

$$\mathbf{F}_{i,j}^{P} = \begin{cases} 0 & \text{for } d_{i,j} > R_i + R_j + \rho \\ \dfrac{1}{\varepsilon_p}(\mathbf{X}_i - \mathbf{X}_j)(R_i + R_j + \rho - d_{i,j})^2, & \text{for } d_{i,j} < R_i + R_j + \rho \end{cases} \tag{12}$$

where $d_{i,j}$ is the distance between the centers of the ith and jth particles, R_i is radius of the ith particle and ρ is the force range, and ε_p is a small positive stiffness parameter. The repulsive force between the particles and the wall is given by

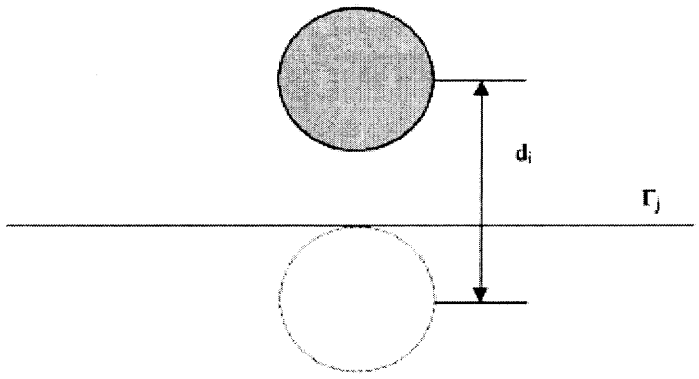

Figure 4.2 The imaginary particle used for computing the repulsive force acting between a particle and a wall.

$$F_{i,j}^{W} = \begin{cases} 0 & \text{for } d_i > 2R_i + \rho \\ \dfrac{1}{\varepsilon_w}(\mathbf{X}_i - \mathbf{X}_j)(2R_i + \rho - d_i)^2, & \text{for } d_i < 2R_i + \rho \end{cases} \qquad (13)$$

where d_i is the distance between the centers of the ith particle and the imaginary particle on the other side of the wall Γ_j, and ε_w is another small positive stiffness parameter (Figure 4.2). The above particle-particle repulsive forces and the particle-wall repulsive forces are added to equation to obtain

$$M_i \frac{dU_i}{dt} = M_i \mathbf{g} + \mathbf{F}_i + \mathbf{F}_i'$$

where

$$\mathbf{F}_i' = \sum_{\substack{j=1 \\ j \neq i}}^{N} \mathbf{F}_{i,j}^{P} + \sum_{j=1}^{4} \mathbf{F}_{i,j}^{W}$$

$\mathbf{F}_i'$ is the repulsive force exerted on the ith particle by the other particles and the walls. In the simulations, ρ is equal to one and half times the velocity mesh size, $\varepsilon_w = 10^{-5}$ and $\varepsilon_p = 2\varepsilon_w$. The repulsive force acts only when the distance between the particles is smaller than ρ.

4.3 Weak Form

The approach used in Glowinski et al. (1997) and Glowinski et al. (1998) is followed for obtaining the weak form of the governing equations stated in the previous section. The only additional complication being that the fluid is viscoelastic, and thus it is also needed to solve the constitutive equation along with the other equations. In obtaining this weak form, the hydrodynamic forces and torques acting on the particles can be completely eliminated by combining the fluid and particle equations of motion into a single weak equation of motion for the combined fluid-particle system. This total momentum equation for the fluid-particle systems was first introduced by Hesla (1991). For simplicity, it is assumed that there is only one particle. The extension to the many-particle case is straightforward.

To state the combined weak form for the equation of motion, the following two spaces needed:

$$\overline{V}_{u\Gamma}(t) = \{(\mathbf{v},\mathbf{V},\xi) \mid \mathbf{v} \in H^1(\Omega)^2, \mathbf{V} \in \mathbf{R}^2, \xi \in \mathbf{R}, \mathbf{v} = \mathbf{V} + \xi \times \mathbf{r} \quad \text{in P(t)}, \quad \text{and } \mathbf{v} = \mathbf{u}_\Gamma(t) \text{ on } \Gamma\},$$

$$\overline{V}_0(t) = \{(\mathbf{v},\mathbf{V},\xi) \mid \mathbf{v} \in H^1(\Omega)^2, \mathbf{V} \in \mathbf{R}^2, \xi \in \mathbf{R}, \mathbf{v} = \mathbf{V} + \xi \times \mathbf{r} \quad \text{in P(t)}, \quad \text{and} \quad \mathbf{v} = 0 \text{ on } \Gamma\}, \quad (14)$$

where R denotes the set of real numbers. The extended fluid-particle velocity (u, U, ω) lie in $\overline{V}_{u\Gamma}$, and the equation of motion in Ω is

$$\int_\Omega \rho_L \left(\frac{d\mathbf{u}}{dt} - \mathbf{g}\right) \cdot \mathbf{v} dx + \left(1 - \frac{\rho_L}{\rho_d}\right)\left(M\left(\frac{d\mathbf{U}}{dt} - \mathbf{g}\right) \cdot \mathbf{V} + I\frac{d\omega}{dt}\xi\right) - \mathbf{F}^{'}.\mathbf{V} = \int_\Omega \sigma : \mathbf{D}[\mathbf{v}] dx, \text{ for all (v, V, } \xi)$$

$\in \overline{V}_0$,

where $\sigma = -p\, I + 2\eta D$ is the stress tensor.

In the above equation the solution u and variation v are required to satisfy the strong form of the constraint of rigid body motion throughout P(t). In the distributed Lagrange multiplier method this constraint is removed from the velocity space and enforced weakly as a side constraint using a distributed Lagrange multiplier term. It was shown that the following weak formulation of the problem holds in the extended domain

For a.e. t>0, find $u \in \overline{W}_{u\Gamma}$, $p \in L_0^2(\Omega)$, $\lambda \in \Lambda(t)$, $U \in R^2$, and $\omega \in R$, satisfying

$$\int_\Omega \rho_L\left(\frac{d\mathbf{u}}{dt}-\mathbf{g}\right)\cdot\mathbf{v}d\mathbf{x} - \int_\Omega p\nabla.\mathbf{v}\,d\mathbf{x} + \int_\Omega 2\eta\mathbf{D}[\mathbf{u}]:\mathbf{D}[\mathbf{v}]d\mathbf{x}$$
$$+\left(1-\frac{\rho_L}{\rho_d}\right)\left(M\left(\frac{d\mathbf{U}}{dt}-\mathbf{g}\right)\cdot\mathbf{V} + I\frac{d\omega}{dt}\xi\right) - \mathbf{F}^{'}.\mathbf{V} = \left\langle\lambda, \mathbf{v}-(\mathbf{V}+\xi\times\mathbf{r})\right\rangle_{P(t)} \tag{15}$$

for all $v \in \overline{W}_0$, $V \in R^2$, and $\xi \in R$,

$$\int_\Omega q\nabla.\mathbf{u}\,d\mathbf{x} = 0 \qquad \text{for all } q \in L^2(\Omega), \tag{16}$$

$$\left\langle\mu, \mathbf{u}-(\mathbf{U}+\omega\times\mathbf{r})\right\rangle_{P(t)} = 0 \qquad \text{for all } \mu \in \Lambda(t), \tag{17}$$

$$\mathbf{u}|_{t=0} = \mathbf{u}_o \qquad \text{in } \Omega, \tag{18}$$

as well as the kinematic equations and the initial conditions for the particle linear and angular velocities. Here,

$$\overline{W}_{u\Gamma} = \{\mathbf{v} \in H^1(\Omega)^2 \mid \mathbf{v}=\mathbf{u}_\Gamma(t) \quad \text{on} \quad \Gamma\},$$

$$\overline{W}_0 = H_0^1(\Omega)^2,$$

$$L_0^2(\Omega) = \{q \in L^2(\Omega) \mid \int_\Omega q\,d\mathbf{x} = 0\} \tag{19}$$

and $\Lambda(t)$ is $H^1(P(t))^2$, with $\langle .,. \rangle_{P(t)}$ denoting the H^1 inner product over the particle. In the simulations, since the velocity and μ are in H^1, the following H^1 inner product is used

$$\left\langle\mu, \mathbf{v}\right\rangle_{P(t)} = \int_{P(t)} \left(\mu.\mathbf{v} + R^2\nabla\mu:\nabla\mathbf{v}\right)d\mathbf{x}, \tag{20}$$

where R is the particle radius.

4.4 Strong Form

The strong form for the weak formulation of (15-18) can be obtained by integrating the stress term by parts. The resulting equations inside the region occupied by the fluid $\Omega\backslash\overline{P(t)}$ are

$$\rho_L\left[\frac{\partial \mathbf{u}}{\partial t}+\mathbf{u}\cdot\nabla\mathbf{u}\right] = \rho_L g -\nabla p+\nabla.(2\eta D)$$

$$\nabla.u = 0$$

$$u = u_L \qquad \text{on } \Gamma$$

$$u = U_i + \omega_i \times r_i \qquad \text{on } \partial P_i(t),\ i=1,\ldots,N$$

and the equations inside the region occupied by the particles P(t) are

$$\rho_L\left[\frac{\partial \mathbf{u}}{\partial t}+\mathbf{u}.\nabla\mathbf{u}\right] = \rho_L g - \nabla p +\nabla.(2\eta D) + \lambda - R^2\nabla^2\lambda$$

$$u = U_i + \omega_i \times r_i \qquad \text{on } \partial P_i(t),\ i=1,\ldots,N, \quad (21)$$

The fact used here is that the rigid body motion satisfies the incompressibility constraint and that the stress inside the particles is zero. The boundary condition on the interface between the fluid and particle regions $\partial P(t)$ is

$$\mathbf{n}.(-\sigma_L) = \mathbf{n}.\nabla\lambda \qquad (22)$$

where n is the normal at the fluid-particle interface, and $\sigma_L = -pI + 2\eta D$ is the stress in the fluid phase, and $\sigma_P = 0$ is the stress inside the particles. For given U(t) and $\omega(t)$, and the positions $X_i(t)$, i=1,..., N, equation (26) can be written as:

$$\boldsymbol{\lambda} - R^2\nabla^2\boldsymbol{\lambda} = \rho_L\left(\frac{d\mathbf{U}}{dt} + \frac{d\boldsymbol{\omega}}{dt}\times\mathbf{r} + \boldsymbol{\omega}\times(\boldsymbol{\omega}\times\mathbf{r}) - \mathbf{g}\right) \tag{23}$$

4.5 Finite-Element approximation

In order to solve the above problem numerically, the domain is discretized using a regular finite element triangulation T_h for the velocity, where h is the mesh size, and a regular triangulation T_{2h} for the pressure. The following finite dimensional spaces are defined for approximating $\overline{W}_{u\Gamma}$, $\overline{W}_0$, $L^2(\Omega)$ and $L^2_0(\Omega)$:

$$W_{u\Gamma,h} = \{\mathbf{v}_h \in C^0(\overline{\Omega})^2 \mid \mathbf{v}_h|_T \in P_1\times P_1 \text{ for all } T\in T_h,\ \mathbf{v}_h = \mathbf{u}_{\Gamma,h} \text{ on } \Gamma\}$$

$$W_{0,h} = \{\mathbf{v}_h \in C^0(\overline{\Omega})^2 \mid \mathbf{v}_h|_T \in P_1\times P_1 \text{ for all } T\in T_h,\ \mathbf{v}_h = 0 \text{ on } \Gamma\} \tag{24}$$

$$L^2_h = \{q_h \in C^0(\overline{\Omega}) \mid q_h|_T \in P_1 \text{ for all } T\in T_{2h}\}$$

$$L^2_{0,h} = \{q_h \in L^2_h \mid \int_\Omega q_h\, d\mathbf{x} = 0\} \tag{25}$$

Using these finite dimensional spaces, the following finite-element approximation to the problem (15)-(18) is obtained

Find $u_h \in W_{u\Gamma,h}$, $p_h \in L^2_{0,h}$, $\lambda_h \in \Lambda_h(t)$, $U \in R^2$, and $\omega \in R$, satisfying

$$\int_\Omega \rho_L\left(\frac{d\mathbf{u}_h}{dt}-\mathbf{g}\right).\mathbf{v}_h d\mathbf{x} - \int_\Omega p_h \nabla.\mathbf{v}_h\, d\mathbf{x} + \int_\Omega 2\eta \mathbf{D}[\mathbf{u}_h]:\mathbf{D}[\mathbf{v}_h]d\mathbf{x}$$
$$+\left(1-\frac{\rho_L}{\rho_d}\right)\left(M\left(\frac{d\mathbf{U}}{dt}-\mathbf{g}\right).\mathbf{V}+I\frac{d\omega}{dt}\xi\right)-\mathbf{F}'.\mathbf{V}=\left\langle \lambda_h, \mathbf{v}_h-(\mathbf{V}+\xi\times\mathbf{r})\right\rangle_{P(t)}$$

for all $v_h \in W_{0,h}$, $V \in R^2$, and $\xi \in R$,

$$\int_\Omega q_h \nabla.\mathbf{u}_h\, d\mathbf{x} = 0 \qquad \text{for all } q_h \in L_h^2,$$

$$\left\langle \mu_h, \mathbf{u}_h-(\mathbf{U}+\omega\times\mathbf{r})\right\rangle_{P(t)} = 0 \qquad \text{for all } \mu_h \in \Lambda_h(t),$$

$$\mathbf{u}|_{t=0} = \mathbf{u}_{0,h} \qquad \text{in } \Omega, \qquad (26)$$

In numerical scheme, since the motion inside the particles is rigid body like, the value of configuration tensor inside the particles is explicitly constrained to be equal to I.

4.6 Time Discretization Using the Marchuk-Yanenko Operator Splitting Scheme

The initial value problem (26) is solved by using the Marchuk-Yanenko operator splitting scheme which allows us to decouple its three primary difficulties:

- The incompressibility condition, and the related unknown pressure p_h,
- The nonlinear advection term,
- The constraint of rigid-body motion in $P_h(t)$, and the related distributed Lagrange multiplier λ_h,

The Marchuk-Yanenko operator splitting scheme can be applied to an initial value problem of the form

$$\frac{d\phi}{dt} + A_1(\phi) + A_2(\phi) + A_3(\phi) + A_4(\phi) = f$$

where the operators A_1, A_2, A_3, and A_4 can be multiple-valued. Let Δt be the time step, and α, β and γ be three constants: $0 \le \alpha, \beta, \gamma \le 1$ and $\alpha + \beta + \gamma = 1$. The following version of the Marchuk-Yanenko operator splitting to simulate the motion of particles in a viscoelastic fluid is used:

Set $u^0 = u_{0,h}$, $U^0 = U_0$, $X^0 = X_0$ and $\omega^0 = \omega_0$.

For n=0,1,2,... assuming u^n, A^n, U^n, X^n, and ω^n are known, find the values for n+1 using the following:

Step 1

Find $u^{n+1/4} \in W^{n+1}_{u\Gamma,h}$ and $p^{n+1/4} \in L^2_{0,h}$, by solving

$$\int_\Omega \rho_L \frac{\mathbf{u}^{n+1/4} - \mathbf{u}^n}{\Delta t}.\mathbf{v}\, d\mathbf{x} - \int_\Omega p^{n+1/4} \nabla.\mathbf{v}\, d\mathbf{x} + \alpha \int_\Omega 2\eta_s \mathbf{D}[\mathbf{u}^{n+1/4}] : \mathbf{D}[\mathbf{v}] d\mathbf{x} = 0$$

for all $v \in W_{0,h}$,

$$\int_\Omega q \nabla.\mathbf{u}^{n+1/4} d\mathbf{x} = 0 \qquad \text{for all } q \in L^2_h, \qquad (27)$$

Step 2

Find $u^{n+2/4} \in W^{n+1}_{u\Gamma,h}$, by solving

$$\int_\Omega \rho_L \frac{\mathbf{u}^{n+2/4} - \mathbf{u}^{n+1/4}}{\Delta t}.\mathbf{v} d\mathbf{x} + \int_\Omega \rho_L (\mathbf{u}^{n+2/4}.\nabla \mathbf{u}^{n+2/4}).\mathbf{v}\, d\mathbf{x} + \beta \int_\Omega 2\eta_s \mathbf{D}[\mathbf{u}^{n+2/4}] : \mathbf{D}[\mathbf{v}] d\mathbf{x} = 0$$

for all $v \in W_{0,h}$ (28)

Step 3

Compute $U^{n+2/4}$ and $X^{n+2/4}$ using the prediction procedure

Set $U^{n,0} = U^n$, $X^{n,0} = X^n$.

Do k=1,K

$$U^{*n,k} = U^{n,k-1} + \left(\mathbf{g} + \left(1 - \frac{\rho_L}{\rho_d} \right)^{-1} M^{-1} F'(X^{n,k-1}) \right) \frac{\Delta t}{K}$$

$$X^{*n,k} = X^{n,k-1} + \left(\frac{\mathbf{U}^{n,k-1} + \mathbf{U}^{*n,k}}{2} \right) \frac{\Delta t}{K}$$

$$U^{n,k} = U^{n,k-1} + \left(\mathbf{g} + \left(1 - \frac{\rho_L}{\rho_d} \right)^{-1} M^{-1} \frac{F'(X^{n,k-1}) + F'(X^{*n,k-1})}{2} \right) \frac{\Delta t}{K}$$

$$X^{n,k} = X^{n,k-1} + \left(\frac{\mathbf{U}^{n,k-1} + \mathbf{U}^{n,k}}{2} \right) \frac{\Delta t}{K}$$

end do

Set $U^{n+2/4} = U^{n,K}$, $X^{n+2/4} = X^{n,K}$. (29)

Find $u^{n+1} \in W^{n+1}_{u\Gamma,h}$, $\lambda^{n+1}_{\cdot} \in \Lambda_h((n+2/4)\Delta t)$, $U^{n+1} \in R^2$, and $\omega^{n+1}_{\cdot} \in R$, satisfying

$$\int_\Omega \rho_L \frac{\mathbf{u}^{n+1}-\mathbf{u}^{n+2/4}}{\Delta t}.\mathbf{v}\,d\mathbf{x} + \left(1-\frac{\rho_L}{\rho_d}\right)\left(M\frac{\mathbf{U}^{n+1}-\mathbf{U}^{n+2/4}}{\Delta t}.\mathbf{V} + I\frac{\omega^{n+1}-\omega^{n+2/4}}{\Delta t}\xi\right) +$$
$$\gamma\int_\Omega 2\eta_s \mathbf{D}[\mathbf{u}^{n+1}]:\mathbf{D}[\mathbf{v}]d\mathbf{x} = \left\langle \boldsymbol{\lambda}^{n+1}, \mathbf{v}-(\mathbf{V}+\xi\times\mathbf{r}^{n+2/4})\right\rangle_{P((n+2/4)\Delta t)}$$

for all $v \in W_{0,h}$, $V \in R^2$, and $\xi \in R$

$$\left\langle \boldsymbol{\mu}_h, \mathbf{u}^{n+1}-(\mathbf{U}^{n+1}+\omega^{n+1}\times\mathbf{r})\right\rangle_{P((n+2/4)\Delta t)} = 0 \quad \text{for all } \boldsymbol{\mu}_h \in \Lambda((n+2/4)\Delta t) \tag{30}$$

where the center of particle $P((n+2/4)\Delta t)$ is at $X^{n+2/4}$.

Set $X^{n+1,0} = X^n$.

Do k=1,K

$$X^{*n+1,k} = X^{n+1,k-1} + \left(\frac{\mathbf{U}^n + \mathbf{U}^{n+1}}{2}\right)\frac{\Delta t}{K}$$

$$X^{n,k} = X^{*n,k-1} + \left(1-\frac{\rho_L}{\rho_d}\right)^{-1} M^{-1}\left(\frac{F'(X^{n+1,k-1}) + F'(X^{*n+1,k})}{2}\right)\frac{(\Delta t)^2}{2K}$$

end do

Set $X^{n+1} = X^{n+1,K}$. (31)

Set $p^{n+1} = p^{n+1/4}$, and go back to the first step.

4.7 Remarks

1. The first step gives rise to a Stokes-like problem for the velocity and pressure distributions which is solved by using a conjugate gradient method (Bristeau et al. 1987)
2. The second step is a nonlinear problem for the velocity which is solved by using a least square conjugate gradient algorithm (Bristeau et al.1987)
3. The third step is used to obtain the distributed Lagrange multiplier that enforces rigid body motion inside the particles. This problem is solved by using a conjugate gradient method described by Glowinski et al. (1997) and Glowinski et al. (1998). In the implementation of the method, an H^1 inner product, expressed in Eq. (20), is used for obtaining the distributions over the particles, as the discretized velocity is in H^1.

CHAPTER 5

RESULTS AND DISCUSSION

5.1 Time History of Different Cases

The objective of this study is to investigate the factors that govern the formation and stability of dense phase slugs in pressure driven flows by direct numerical simulations. In a pressure driven flow the lift forces, which keep particles suspended, arise both due to particle-particle interaction and the shearing nature of the flow. In this work, initially, the particles are placed close to each other so that they can form a slug, as in the dense phase conveying of the powders covering the full domain in the y-direction and 50% in the x-direction, leaving enough space above the particles to get lifted as the flow develops.

The gravity acts in the negative x-direction while the direction of the flow is in negative z-direction as shown in the Figure 5.1(a). Several cases were investigated based on the different pressure gradient values and different densities of the particles.

Following is the system of units used for this study.

Quantity	Units
Length	cm
Time	sec
Pressure Gradient	dyn/cm^3
Viscosity	poise
Density	g/cm^3

Table 5.1 Units for dimensional quantities.

5.2 Normal Gravity Case (A)

In case (A) the pressure gradient applied is 100 dyn/cm^3 and the density of particles is 1.01 g/cm^3 where as that of the fluid is 1.0 g/cm^3. When the flow is started three different layers of the particles based on their motion in the fluid are observed;

1. The particles present at the center of the domain (top of the slug) move faster as the flow is parabolic. These particles have a greater tendency to lift up (in positive x-direction) under the action of the shear forces acting on the particles.
2. The particles at the bottom of the slug move with negligible velocity forming the static layer of the slug. Theses particles also have a potential to lift up as described by Hu (1999), but due to their weight acting downward and interaction forces of the particles above, they are not lifted up. But as the particles above pass them, some of the particles are lifted to the upper layer as long as they are not again pressed downward due to the factors described above. These particles are slow in their movement because of the friction between the particles and walls near to them.
3. The particles in between these two layers form the third layer. These particles can be considered to just rolling on top of the particles of the second layer. These particles move with almost constant velocities.

The center of mass is calculated by using the formula,

$$Center\ of\ mass\ of\ Slug = \frac{\sum_{i=1}^{n} x_i}{n}$$

where x_i = x-coordinate of the ith particle.

n = Number of particles.

The Reynolds number for each case is calculated using the following formula for two-dimensional flows,

$$Re = \frac{R\ h^2}{8\mu^2} * \frac{dp}{dx}$$

where, R = Radius of a particle.
h = Height of the channel.
dp/dx = Pressure gradient applied.
μ = Viscosity of the fluid.

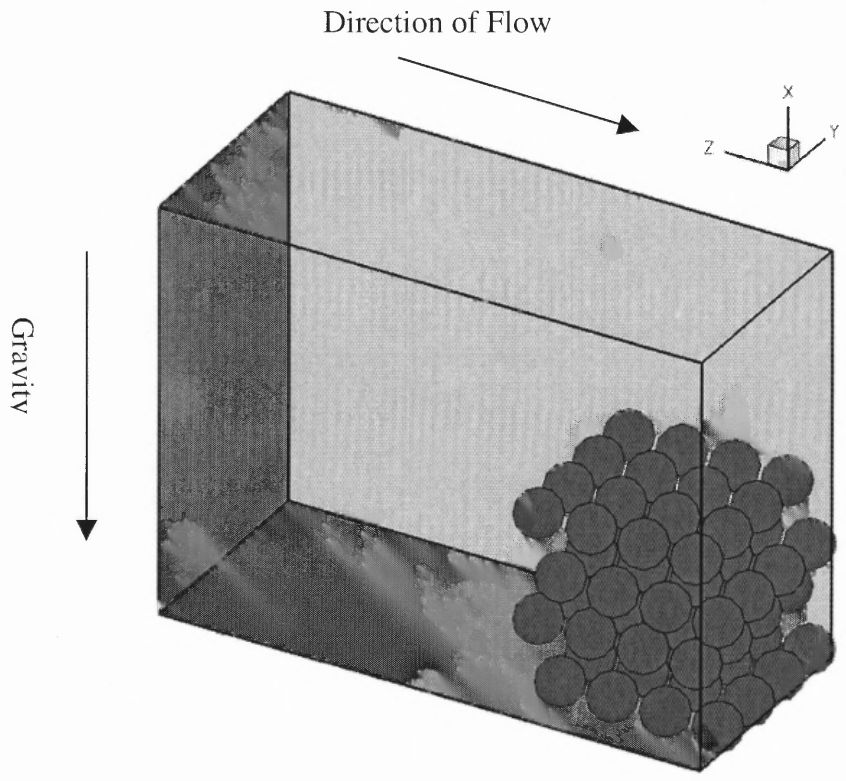

(a)

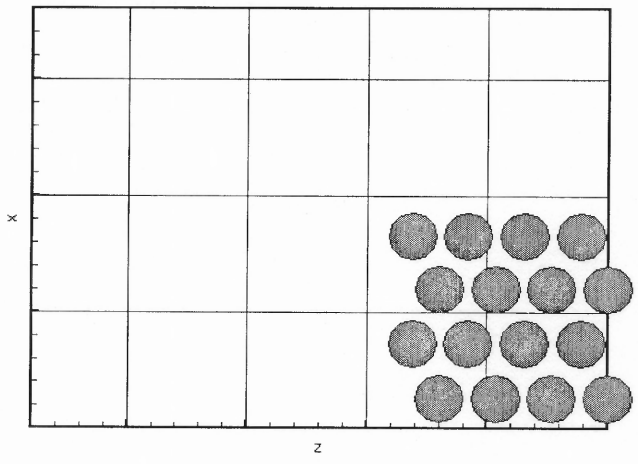

(b)

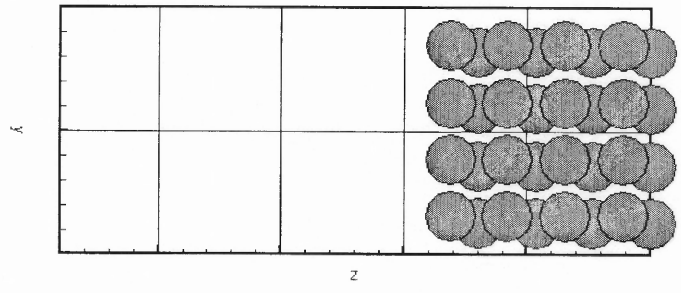

(c)

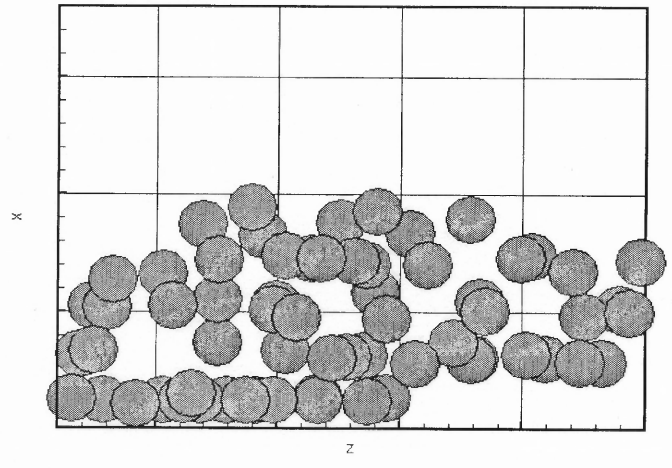

(d)

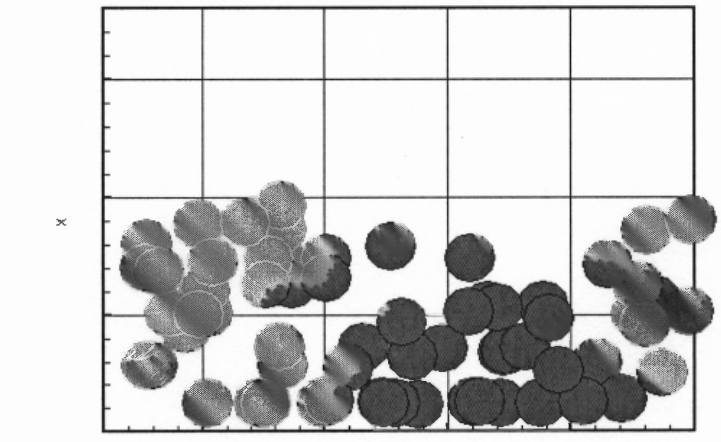

(e)

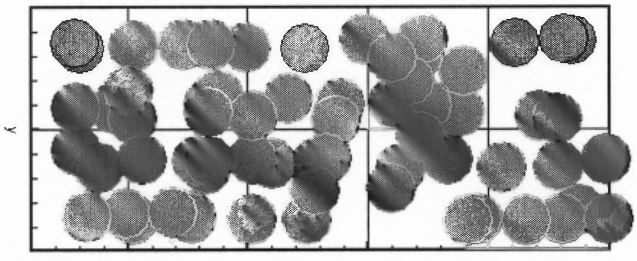

(f)

Figure 5.1 The particle distribution is shown at three different times
(a) The initial position of the particles is shown in the channel.
(b) t = 0 sec.
(c) Figure 5.1(b) in yz-plane.
(d) t = 0.541sec.
(e) t = 0.811 sec.
(f) Figure 5.1(e) in yz-plane.

Reynolds number is calculated as,

$$Re = \frac{0.1*(1.8)^2}{8*(1.0)^2}*100$$

$$Re = 4.05$$

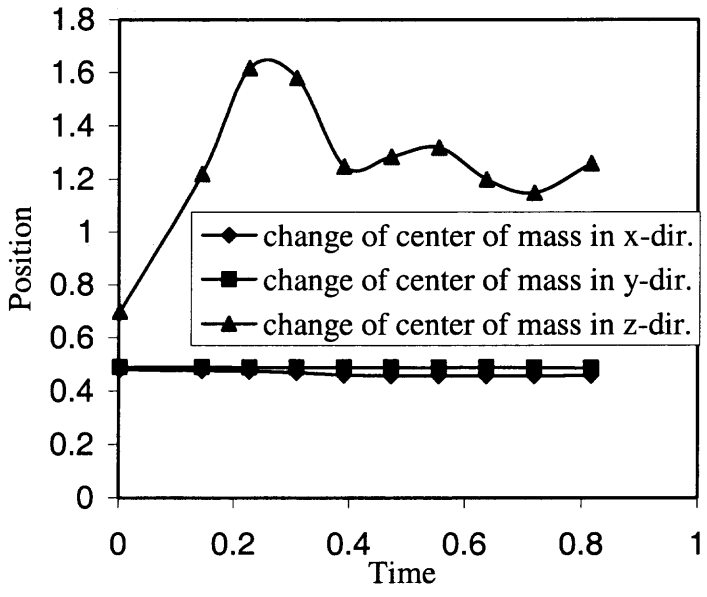

(a)

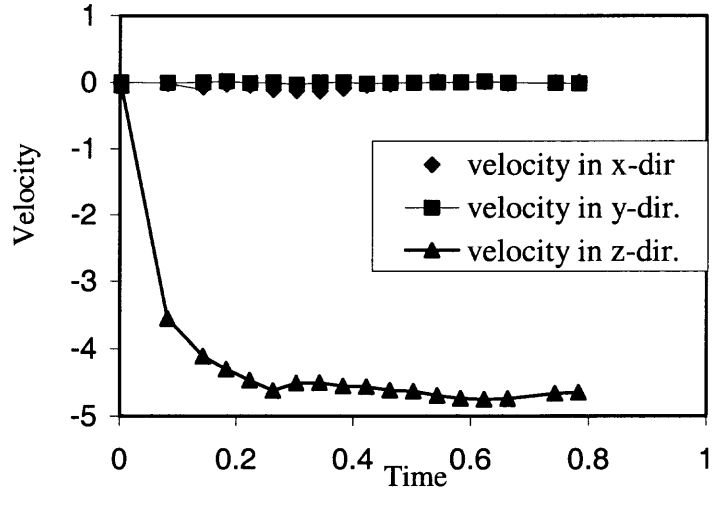

(b)

Figure 5.2 (a) The x, y and z-coordinates of the center of mass of the slug are shown as functions of time.
(b) The x, y and z-components of the translational velocity of the slug are shown as functions of time.

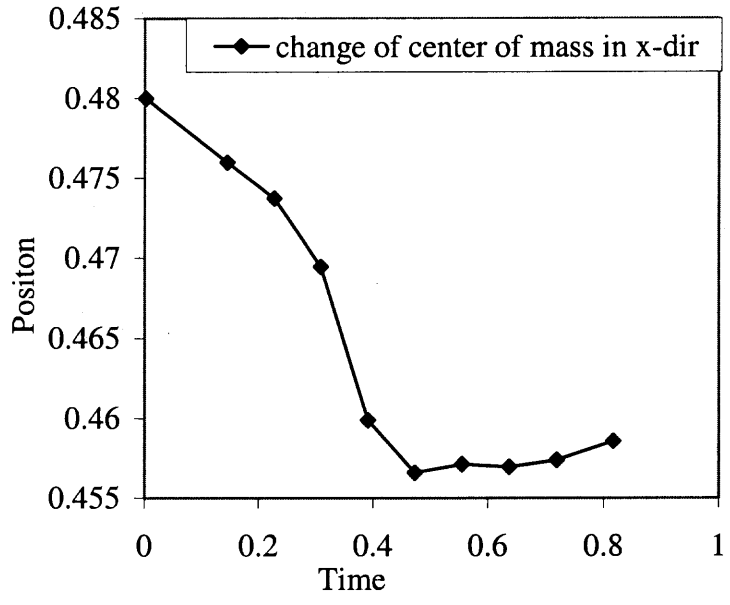

(a)

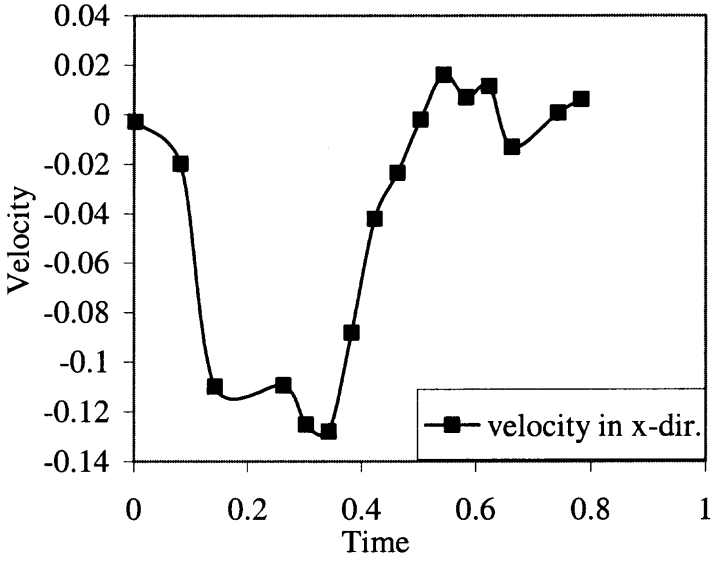

(b)

Figure 5.3 (a) The x-coordinate of the center of mass is shown as a function of time.
(b) The x-component of the translation velocity is shown as a function of time.

The position of the center of mass changes rapidly in the z-direction as the flow develops and at t = 0.2 sec, the flow becomes nearly steady and approximately fully developed and after that there are no significant changes in the velocity.

5.3 Normal Gravity Compact-Configuration Case (B)

In case (B), all the parameters are the same as for case (A) except the particles are placed in different configuration, i.e., in a more compact form and the pressure gradient applied is doubled. Similar kinds of layers were observed as described for case (A) as shown in Figure 5.4

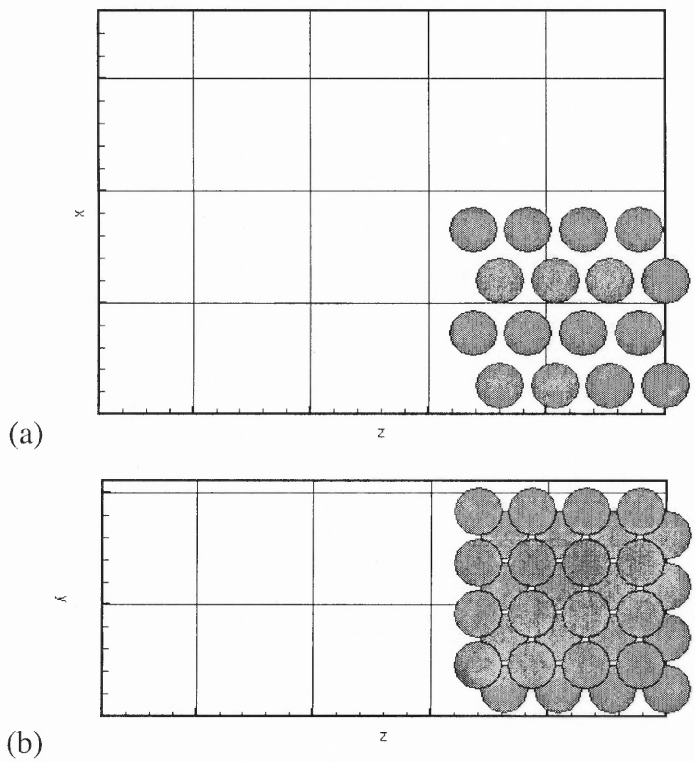

(a)

(b)

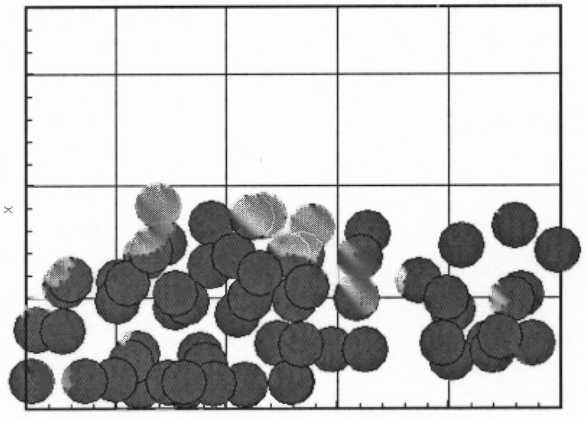

(c)

Figure 5.4 The particle distribution is shown at two different times
(a) t = 0 sec.
(b) Figure 5.4(a) in yz-plane.
(c) t = 0.30705 sec.

Reynolds number is calculated as,

$$Re = \frac{0.1*(1.8)^2}{8*(1.0)^2}*100$$

$$Re = 4.05$$

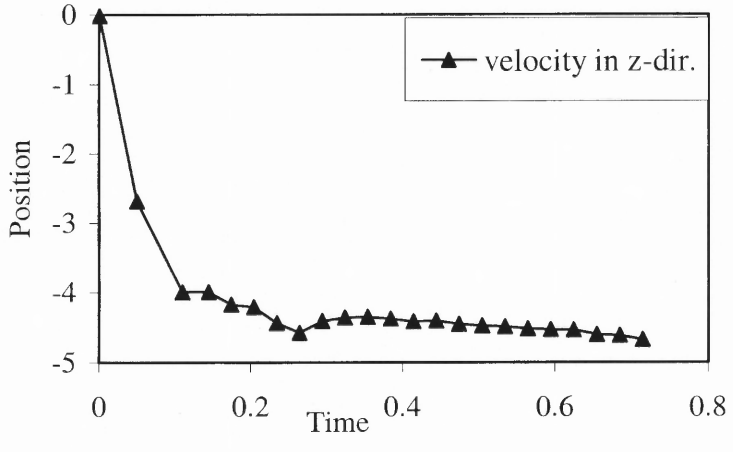

(a)

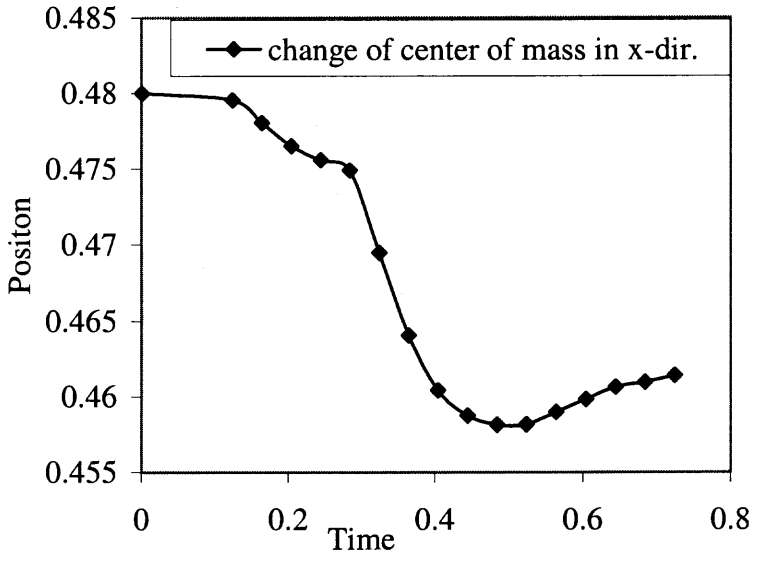

(b)

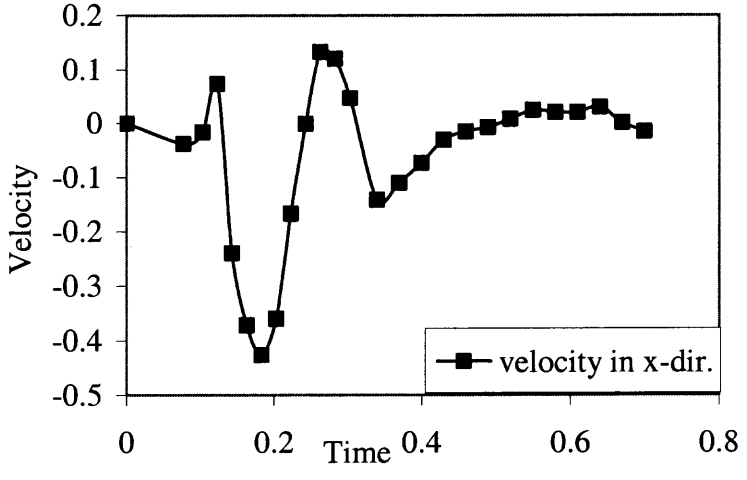

(c)

Figure 5.5 (a) The z-component of the translation velocity is shown as a function of time.
(b) The x-coordinate of the center of mass is shown as a function of time.
(c) The x-component of the translation velocity is shown as a function of time.

In Figure 5.5, the magnitude of slug velocity in the z-direction is nearly the same as for case (A) despite the fact that the pressure gradient is doubled. This is due to the fact that as the initial configuration of the slug is less permeable so a larger pressure gradient is required to cause the flow. However, the point to be noted is that in the Figure 5.5, there is an early increase in the velocity of the slug in the x-direction, i.e., at t = 0.183 sec., while in case (A) the increase in the velocity of the slug in the x-direction occurred at t = 0.343 sec. This result is in agreement with the fact that as the pressure gradient is increased the particles velocities in the flow direction are larger and therefore the lift force which causes the particles to lift against gravity is also larger.

5.4 Reduced Gravity Case (C)

In case (C) the effect of reduced gravity is investigated; the gravity is decreased from 981.0 cm/sec^2 in case (A) to 98.0 cm/sec^2 after t = 0.402 sec.

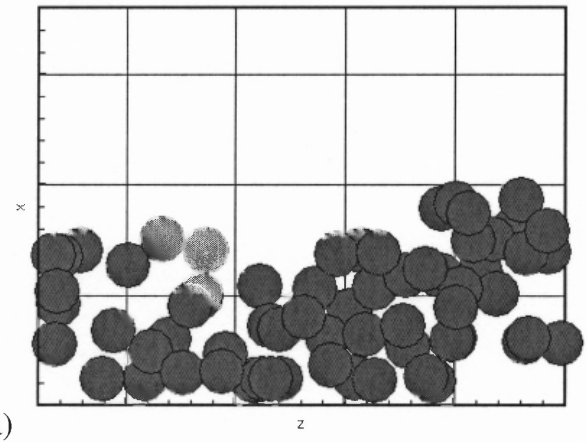

(a)

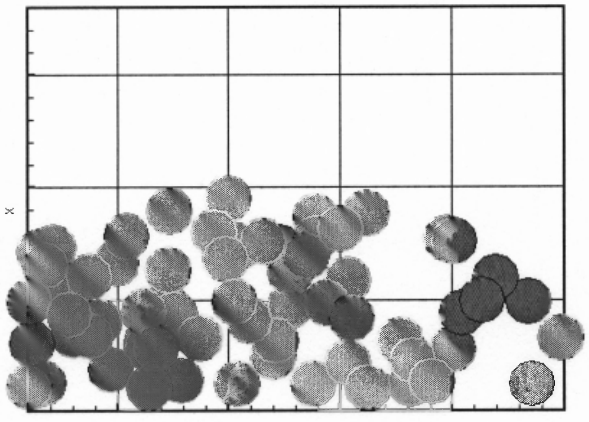

(b)

Figure 5.6 The particle distribution is shown at two different times
(a) t = 0.402 sec. At this time the gravity is reduced from 981.0 cm/sec^2 to 98.0 cm/sec^2
(b) t = 0.54875 sec.

Reynolds number is calculated as,

$$Re = \frac{0.1*(1.8)^2}{8*(1.0)^2}*400$$

$$Re = 16.2$$

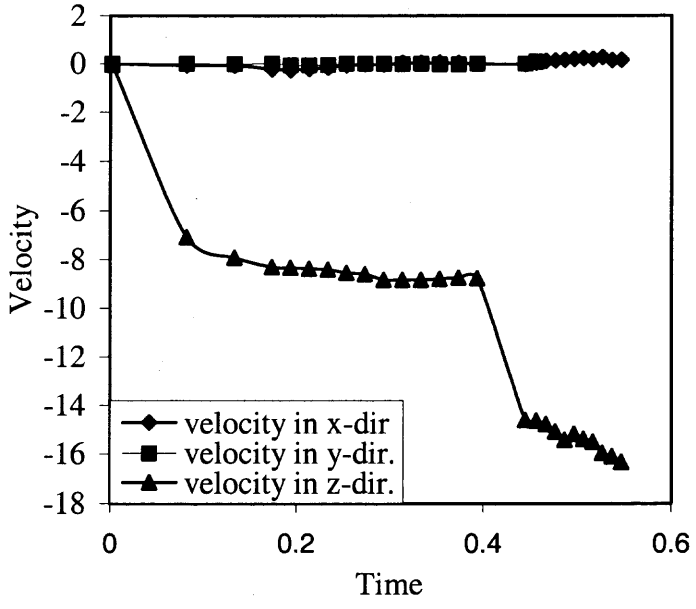

(a)

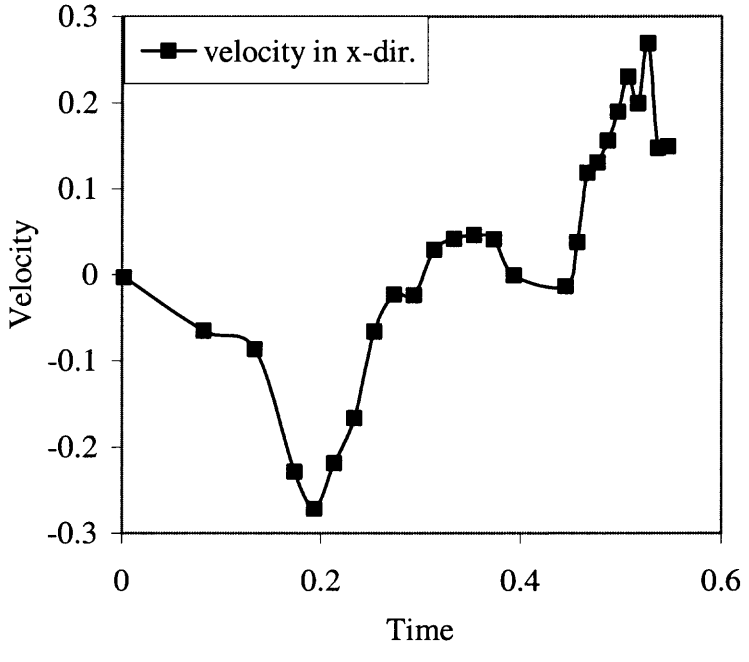

(b)

Figure 5.7 (a) The x, y and z-components of the translation velocity are shown as functions of time.
(b) The x-component of the translation velocity is shown as a function of time.

The effect of this reduction of gravity on the particles is that the particle velocity in the flow direction increases, see Figure 5.7(a), they also experience more lift in the x-direction, as shown in Figure 5.7(b). This result is reasonable because when the gravity is reduced, the particles can be lifted more easily. As a result, the particles experience fewer particle-particle interactions as the distance between them is larger and therefore, the resistance to their free flow is reduced. In addition, shearing nature of the flow also causes the particles to lift.

5.5 Reduced Pressure Gradient Case (D)

In case (D), the pressure gradient is decreased from 400 dyn/cm^3 to 10 dyn/cm^3 after the flow in the channel is nearly fully developed. At this instant the particle density is changed from 1.01 g/cm^3 to 1.1 g/cm^3. The effect of a decrease in the pressure gradient is that the lift acting on them decreases and thus they fall under gravity. The increased particle weight also causes the particles to settle down.

Reynolds number is calculated as,

$$Re = \frac{0.1*(1.8)^2}{8*(1.0)^2}*400$$

$$Re = 16.2$$

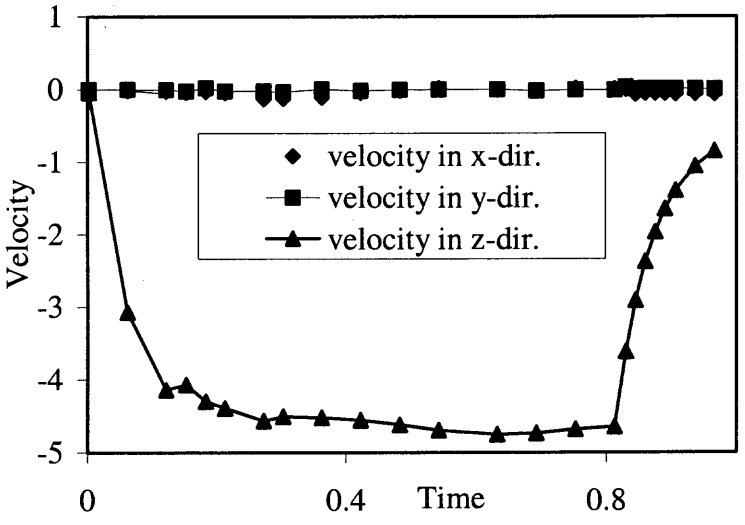

(a)

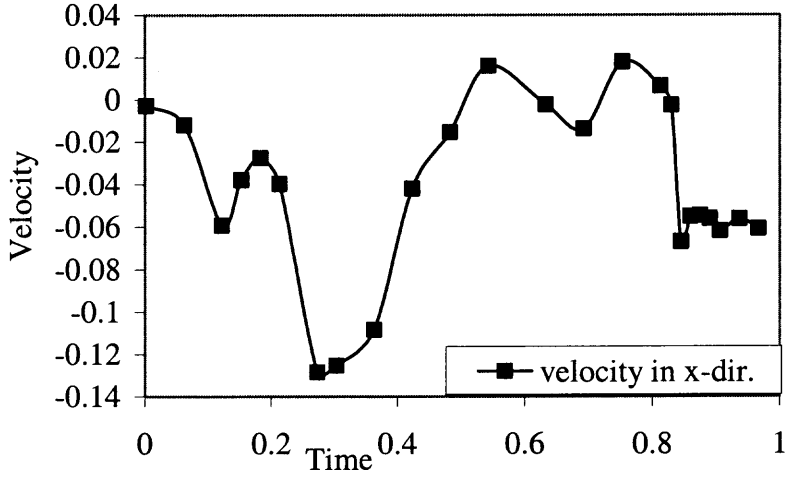

(b)

Figure 5.8 (a) The x, y and z-components of the translation velocity are shown as a function of time.
(b) The x-component of the translation velocity is shown as a function of time.

As it is observed from Figure 5.8 (a), the velocity of the slug decreases quickly in the z-direction as the pressure gradient is reduced suddenly. The behavior of both curves is identically opposite to that in case (C) shown in Figure 5.7 (a), (b) where the particles settle under gravity.

5.6 Increased Viscosity Case (E)

In case (E), the pressure gradient applied is 100 dyn/cm^3 and density of particles is 1.01 g/cm^3 where as that of the fluid is 1.0 g/cm^3. However, the viscosity is increased from 1.0 poise to 5.0 poise.

Reynolds number is calculated as,

$$Re = \frac{0.1*(1.8)^2}{8*(5.0)^2}*100$$

$$Re = 0.162$$

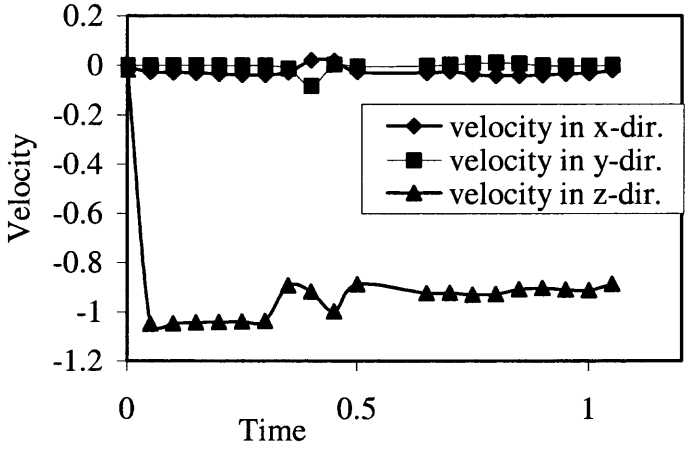

(a)

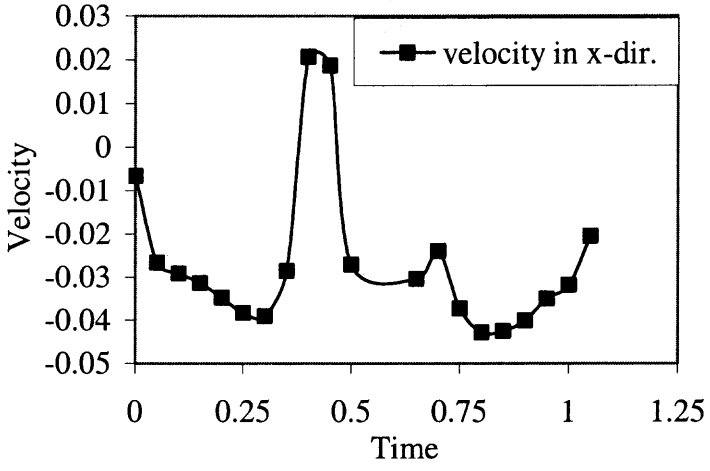
0.03
0.02
0.01
0
-0.01
-0.02
-0.03
-0.04
-0.05
Velocity
velocity in x-dir.
0
0.25
0.5
0.75
1
1.25
Time

(b)

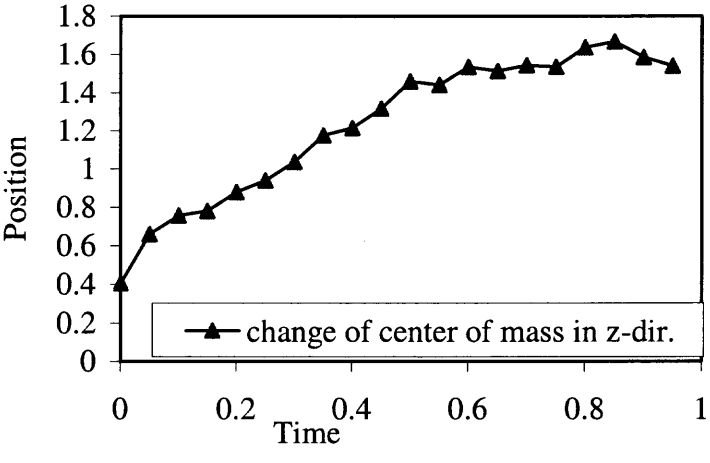
1.8
1.6
1.4
1.2
1
0.8
0.6
0.4
0.2
0
Position
change of center of mass in z-dir.
0
0.2
0.4
0.6
0.8
1
Time

(c)

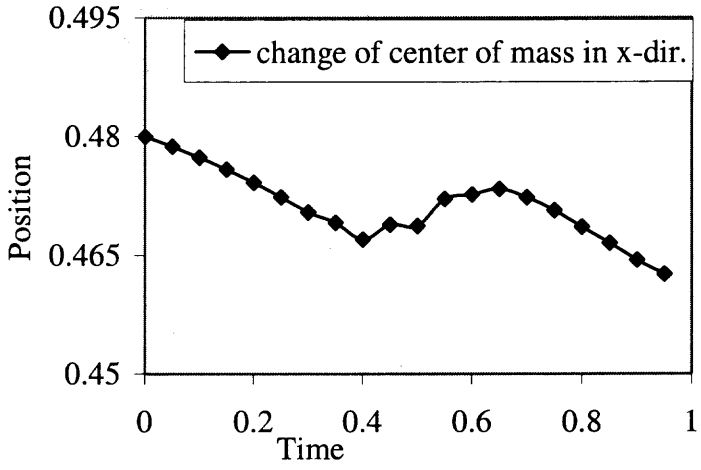

(d)

Figure 5.9 (a) The x, y and z-components of the translation velocity are shown as functions of time.
(b) The x-component of the translation velocity is shown as a function of time.
(c) The z-component of the center of mass is shown as a function of time.
(d) The x-component of the center of mass is shown as a function of time.

The position of the center of mass changes rapidly in the z-direction as the flow develops and at t = 0.6 sec, the flow becomes nearly steady and approximately fully developed and after that there are no significant changes in the velocity.

5.7 Increased Viscosity-Increased Pressure Gradient Case (F)

In case (F), all the parameters are the same as for the case (E) except the pressure gradient is doubled. The viscosity of the fluid is 5.0 poise and the particle density is 1.01 g/cm^3.

Reynolds number is calculated as,

$$Re = \frac{0.1*(1.8)^2}{8*(5.0)^2}*200$$

$$Re = 0.324$$

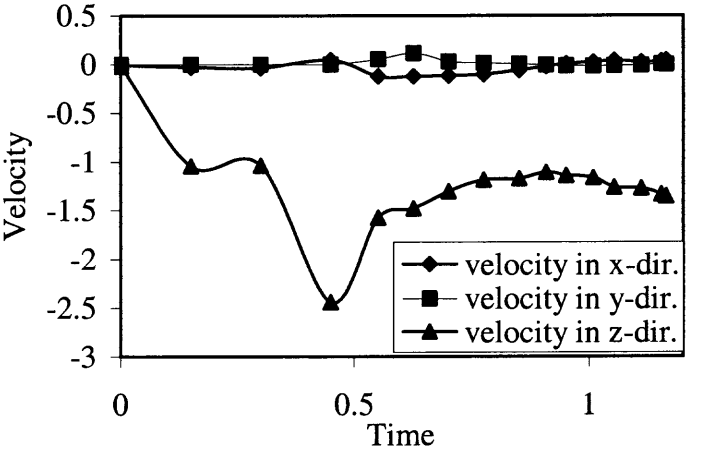

(a)

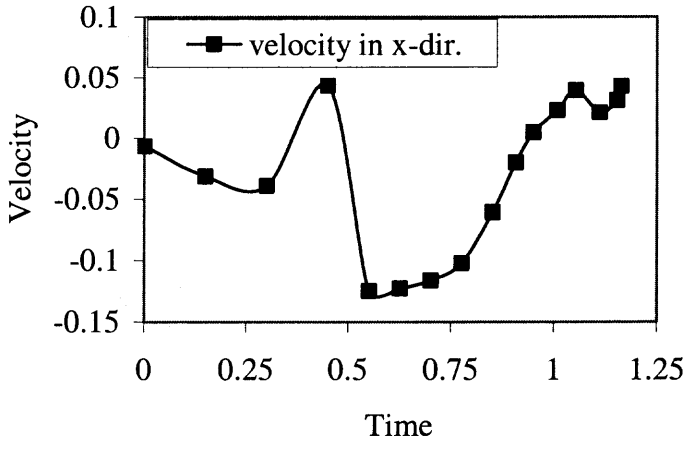

(b)

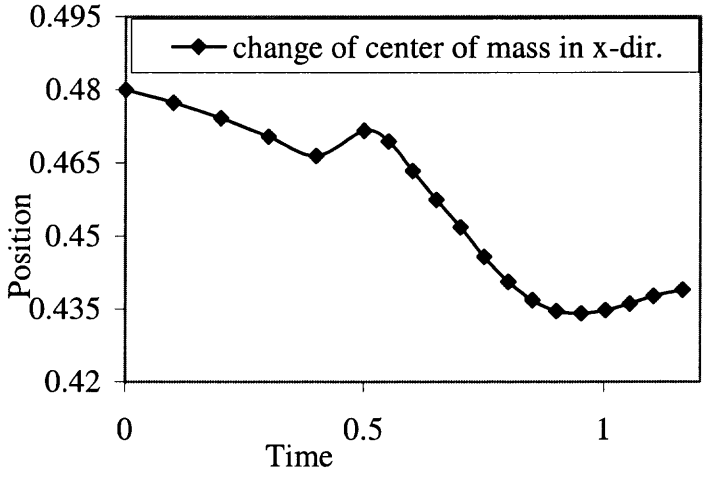

(c)

Figure 5.10 (a) The x, y and z-components of the translation velocity are shown as functions of time.
(b) The x-component of the translation velocity is shown as a function of time.
(c) The x-coordinate of the center of mass is shown as a function of time.

In Figure 5.10, the magnitude of slug velocity in the z-direction is nearly the double as for case (E). This is due to the fact that the pressure gradient applied is also doubled hence it shows the pressure driven nature of the flow. However, the point to be noted is that in the Figure 5.10, there is an early increase in the velocity of the slug in the x-direction, i.e., at t = 0.3 sec, which is approximately the same as for case (E). This result may be due to the fact that as the viscosity of the fluid is increased, it causes most of the particles to settle down and when the particles, flowing in the middle of the channel, comes again on the top of the settling particles, there are more particle-particle interactions which cause the particles to lift.

5.8 Increased Viscosity Case (G)

In case (G), the pressure gradient applied is same as for case (F) but the value of viscosity is doubled. The particle density is 1.01 g/cm^3.

Reynolds number is calculated as,

$$Re = \frac{0.1*(1.8)^2}{8*(10.0)^2}*200$$

$$Re = 0.081$$

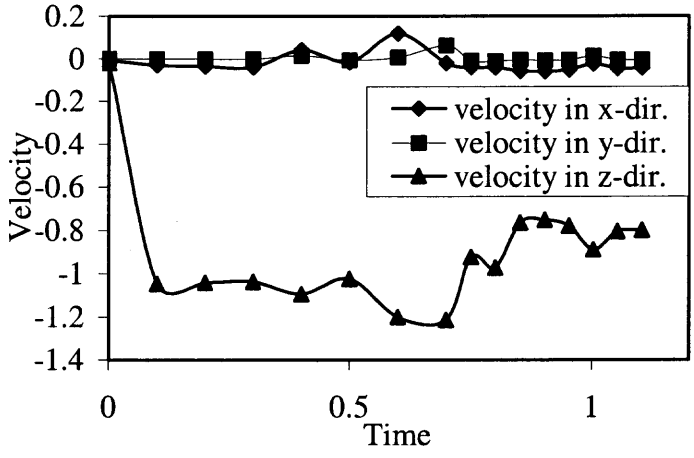
0.2
0
-0.2
-0.4
-0.6
-0.8
-1
-1.2
-1.4
Velocity
0
0.5
1
Time
velocity in x-dir.
velocity in y-dir.
velocity in z-dir.

(a)

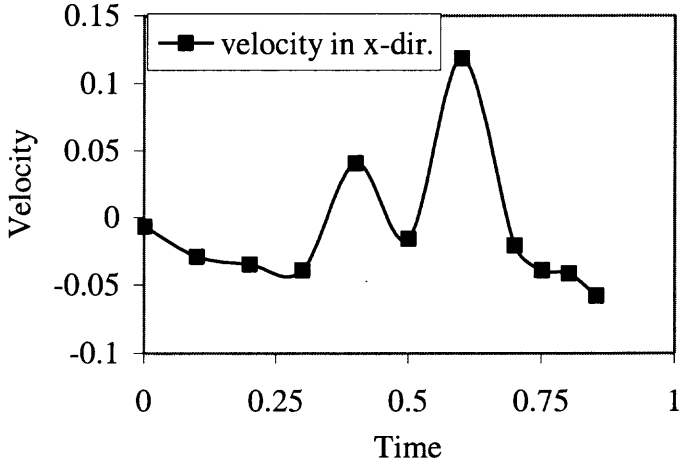
0.15
0.1
0.05
0
-0.05
-0.1
Velocity
0
0.25
0.5
0.75
1
Time
velocity in x-dir.

(b)

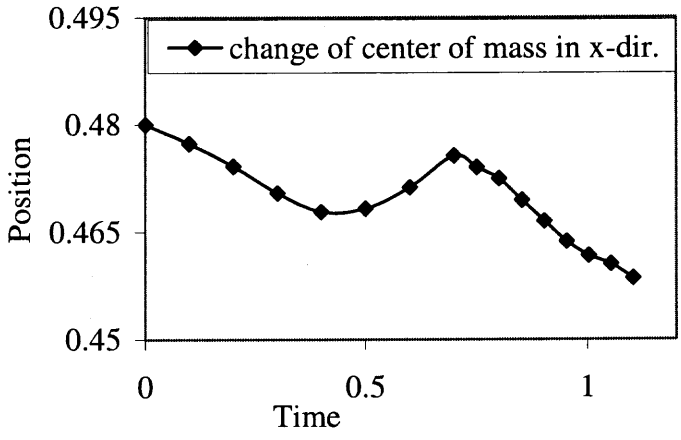

(c)

Figure 5.11 (a) The x, y and z-components of the translation velocity are shown as functions of time.
(b) The x-component of the translation velocity is shown as a function of time.
(c) The x-component of the center of mass is shown as a function of time.

The effect of increase in the fluid viscosity on the particles is that initially the particles start settling down, see Figure 5.11(c), however, at t = 0.5 sec, there are more particle-particle interactions between the flowing particles and the setting particles, due to which the flowing particles experience more lift in the positive x-direction, as shown in Figure 5.11(c). When the flow is nearly developed then the particles again start settling down under gravity. This result is reasonable because when the viscosity is increased, the particles (being heavier than the fluid) settle more easily due to gravity as the fluid velocity, with pressure gradient fixed, is smaller.

CHAPTER 6

CONCLUSIONS

In this work the distributed Lagrange Multiplier/fictitious domain method is used to simulate the motion of slugs in dense phase conveying (Glowinski et al. 1998 and Singh et al. 2000). The governing equations are solved at scales finer than the particle size without the use of any ad hoc two-phase flow model. The ability to numerically simulate the motion of slugs and analyze the parameters that govern the formation and stability of slugs will serve to broaden our understanding of dynamics of motion of slugs in dense phase conveying.

The simulations were started by placing the particles in three dimensional periodic arrays, close enough to form slugs. The behavior of the slugs is then analyzed as a function of the applied pressure gradient, packing density, fluid viscosity, density of fluid and particles and strength of the gravitational field. A summary of results is as follows:

1. Three layers of particles were formed, and while the top layer of the slug moved fast, the bottom layer experienced little to no lift.
2. When the packing density was increased, a higher pressure gradient was required to cause flow.
3. When the strength of the gravitational field was reduced, the particle velocity in the flow direction increased and the particles experienced a greater lift, i.e. the resistance offered by the slug to the flow reduces.

4. When the pressure gradient was reduced after the flow in the channel was fully developed, while simultaneously increasing the particle density, the velocity of the slug in the direction of flow decreased quickly.
5. When the viscosity of the fluid was increased and the pressure gradient is held fixed, the fluid velocity decreases and particles settle under gravity.

REFERENCES

Albright, C. et al., "Pressure Drop in Flow of Dense Coal-Air Mixtures," Industrial and Engineering Chemistry, Vol. 43, No. 8 (1951), pp. 1837-1840.

Alder, B.J. et al., "Statistical Mechanical Theory of Transport Properties." Proceedings of the International Union of Pure and Applied Physics. (1956).

Ashurst, W.T. et. al., "Argon Shear Viscosity Via a Lennard-Jones Potential with Equilibrium and Non-Equilibrium Molecular Dynamics." Physical Review Letters, 31 (1973), pp. 206-209.

Behrendt, U. et al., "The EOS Rapid Prototyping Concept," Computers in Industry, Vol. 28 (1995), pp. 57-61.

Brady, J.F. et al., "Stokesian Dynamics." Ann. Rev.Fluid Mech., 20 (1988), pp.111-157.

Bristeau, M.O. et al., "Numerical Methods for the Navier-Stokes Equations. Applications to the Simulation of Compressible and Incompressible Flows." Computer Physics Reports, 6 (1987), pp. 73-187.

Brown, R. et al., "Principles of Powder Mechanics," P. Danchwerts (ed.), Pergamon Press, (1970), pp. 1-12.

Carpinlioglu, M.O. et al., "An Experimental Approach for the Determination of Development Length in Particulate Flows." Int. J. Multiphase Flow, Vol. 24, No. 2 (1998), pp. 347-353.

Dickson, A. et al., "Plug Phase Conveying," Proceedings of Pneumotransport, 4 (1978).

Dippel, S. et al., "Simulations on Size Segregation: Geometrical Effects in the Absence of Convection." J. Phys. I France, 5 (1995), pp. 1527.

Fitzgerald, S. et al., "A Pneumatic Conveying Powder Delivery System For Continuously Heterogeneous Material Deposition in Solid Freeform Fabrication." MSME thesis, (1996).

Flain, R., "Pneumatic Conveying: How the System is Matched to the Materials," Process Engineering (1972), pp. 88-90.

Geldart, D., "Powder Processing - The Overall View," Principles of Powder Technology, M. Rhodes (ed.), John Wiley and Sons, (1990), pp. 1-8.

Glowinski, R. et al., "Finite Element Methods for Navier-Stokes Equations." Annu. Rev. Fluid Mech. 24 (1992), pp.167-204.

Glowinski, R., et al., "A Lagrange Multiplier-Fictitious Domain Method for the Numerical Simulation of Incompressible Viscous Flow Around Moving Rigid Bodies." C. R. Acad. Sci. Paris, 324 (1997), pp. 361-369.

Glowinski, R., et al., "A Distributed Lagrange Multiplier/Fictitious Domain Method for Particulate Flows." Int. J. of Multiphase Flows, 25 (1998), pp. 755-794.

Hesla, T. I., "The Dynamical Simulation of Two-Dimensional Fluid/Particle Systems." Unpublished Notes (1991).

Hirota, M. et al., "Effect of Mechanical Properties of Powder on Pneumatic Conveying in Inclined Pipe" Powder Technology, Vol.122 (2002), pp. 150-155.

Hong, J. et al., "A Model for Gas-Solid Stratified Flow in Horizontal Dense-Phase Pneumatic Conveying." Powder Technology, Vol. 77 (1993), pp. 107-114.

Hong, J. et al., "Phase Diagrams in Dense Phase Pneumatic Transport". Powder Technology, Vol. 84 (1995), pp. 213-219.

Hu, H.H., "Direct Simulation of Flows of Solid-Liquid Mixtures." Int. J. Multiphase Flow, 22 (1996), pp. 335-352.

Hu, H.H., "Direct Simulation of the Sedimentation of Elliptic Particles in Oldroyd-B Fluids." J. Fluid Mech., 362 (1998), pp. 297-325.

Hu, H.H., "Simulation of Particulate Flows of Newtonian and Viscoelastic Fluids." Third International Conference of Multiphase Flows (1998).

Johnson, K.L., "Contact Mechanics." (1987),Cambridge, Cambridge University Press.

Joseph, D.D., "Fluid Dynamics of Viscoelastic Liquids." (1990), Springer-Verlag, New York.

Kano, T., et al., "A Study of the Optimum Conditions for Plug-Type Pneumatic Conveying of Granular Materials." Intl. Chem. Engr., 24 (1984), pp. 702-709.

Klausner, J.F. et al., "A Fluid Mechanics Approach to Describe the Behavior of Pneumatically Conveyed Powder Plugs." Powder Technology, Vol. 124 (2002), pp. 127-137.

Klinzing, G.E. et al., "Dense Phase Plug Flow Transfer: The 1-Inch Horizontal Flow." Powder Technology, Vol. 62 (1990), pp. 41-49.

Klinzing, G.E., "Plug Flow Transport of Cohesive Coal: Horizontal and Inclined Flows." Powder Technology, Vol. 55 (1988), pp. 97-105.

Konrad, K. et al, "Prediction of the Pressure Drop for Horizontal Dense Phase Pneumatic Conveying of Particles". Pneumotransport, 5 (1980).

Konrad, K. "Dense-Phase Pneumatic Conveying: A Review," Powder Technology, Vol. 49 (1986), pp. 1-35.

Lakshminarayan, U. et al., "An Experimental Study of the Relationship Between Microstructure and Mechanical Properties of a Ceramic Fabricated by Selective Laser Sintering," Proceedings Solid Freeform Fabrication Symposium (1992), pp. 44-53.

Levy, A., "Two-Fluid Approach for Plug Flow Simulations in Horizontal Pneumatic Conveying" Powder Technology, Vol.112 (1998), pp. 263-272.

Lippert, A., "Pneumatic Conveyance of Solids at High Concentrations," Chemie-Ingenieur-Technik, Vol. 38, No. 3 (1966), pp. 350-355.

Lubachevsky, B.D., Journal of Computational Physics, 94 (1991), pp. 255.

Luke, S.P. et al., "Real Time Visualization and Analysis of Dense Phase Powder Conveying." Powder Technology, Vol. 102 (1999), pp. 1-13.

Mason, D.J. et al., "A Simulation System for Pneumatic Conveying System." Powder Technology, Vol. 95 (1998), pp. 7-14.

Mason, D.J. et al., " The Effect of a Bend on the Particle Cross-section Concentration and Segreragtion in Pneumtic Conveying Systems." Powder Technology, Vol. 98 (1998), pp. 95-103.

Mason, D.J. et al., "A Model For Non-Suspension Gas-Solids Flow of the Fine Powders in Pipes." Int. J. Multiphase Flow, Vol. 27 (2001), pp. 415-435.

Matsuda, M. et al., "Dense Phase Flow of Powder In Horizontal and Inclined Pneumatic Conveying by a Nemo Pump." Powder Handling and Processing, Vol 12. No.1 (2000), pp. 17-21.

McKee, S.L. et al., "Solids Flow Imaging and Attrition Studies in a Pneumatic Conveyor." Powder Technology, Vol. 82 (1995), pp. 105-113.

Mindlin, R.D. et al., "Elastic Spheres in Contact Under Varying Oblique Forces" Journal of Applied Mechanics, 20 (1953), pp. 327.

Molerus, O., "Principles of Flow in Disperse Systems." (1993), Chapman-Hall Press.

Muschelknautz, E. et al., Chemie-Ing-Tech, 41 (1969), pp. 1164.

Neuffer, D. et al., "Control of Pneumatic Conveying Using ECT." 1st World Congress on Industrial Process Tomography (1999), pp. 71-76.

Patankar S.V., "Numerical Heat Transfer and Fluid Flow." (1980), McGraw-Hill, New York.

Patankar, N. et al., "A New Formulation of the Distributed Lagrange Multiplier/Fictitious Domain Method for Particulate Flows." International Journal of Multiphase Flows (2001), to appear.

Rosato, A.D. et al., "Particle Dynamics Calculations of Wall Stresses and Slip Velocities for Granular Couette Flow of Smooth Inelastic Spheres." Continuum Mechanics and Thermodynamics, 6(1) (1994), pp. 1-20

Rosato, A.D. et al., "Macroscropic Behavior of Vibrating Beds of Smooth Inelastic Spheres." Physics of Fluids, 7(8) (1995), pp. 1818-1831.

Singh, P. et al., Theoret. Comput. Fluid Dynamics 5 (1993), pp. 107-137.

Singh, P. et al, J. Rheol. 38(3) (1994), pp. 485-517.

Singh, P. et al., "Air Entrainment Effects in Powder Flows." IUTAM Proceedings on Segregation in Granular Flows (1999).

Singh, P. et al., "Sedimentation of a Sphere Near a Vertical Wall in an Oldroyd-B Fluid." J. of Non-Newtonian Fluid Mechanics, 94 (2000), pp. 179-203.

Singh, P. et al., "A Modified DLM/FD Method for Particulate Flows with Collisions." Int. J. Multiphase Flows (2001).

Sundaresan, S., "Some Outstanding Questions in Handling of Cohesionless Particles." Powder Technology, Vol. 115 (2001), pp. 2-7.

Taylor, T., "Specific Energy Consumption and Particle Attrition in Pneumatic Conveying." Powder Technology, Vol. 95 (1998), pp. 1-6.

Tezduyar, T.E. et al., (1992) Minnesota Supercomputer Institute.

Tomita, Y. et al., "Pneumatic Slug Conveying in a Horizontal Pipeline." Powder Technology, Vol. 94 (1997), pp. 229-233.

Vu-Quoc, L. et al., "An Accurate and Efficient Tangential Force-Displacement Model for Elastic Frictional Contact in Particle-Flow Simulations." Mechanics of Materials, 31 (1999), pp. 235-269.

Walton, O.R. et al., "Stress Calculations for Assemblies of Inelastic Spheres in Uniform Shear." Acta Mechanica, 63 (1986), pp. 73.

Walton, O.R., "Viscosity and Temperature Calculations for Assemblies of Inelastic Frictional Disks." Journal of Rheology, 30(5) (1986), pp. 949-980.

Walton, O.R., "Numerical Simulation of Inclined Chute Flows of Monodispers, Inelastic, Frictional Spheres." Second U.S.-Japan Seminar on Micromechanics of Granular Materials (1991).

Weber, N., Stromungs-Fordertechnik (1973), Krausskoph Verlag.

Wypych, P.W. et al., "A Standardized Test Procedure for Pneumatic Conveying Design." Bulk Solids Handling, 5 (4) (1985), pp. 33-41.

Wypych, P.W., et al., "Pressure Drop and Slug Velocity in Low-Velocity Pneumatic Conveying of Bulk Solids". Powder Technology, Vol. 94 (1997), pp. 123-132.